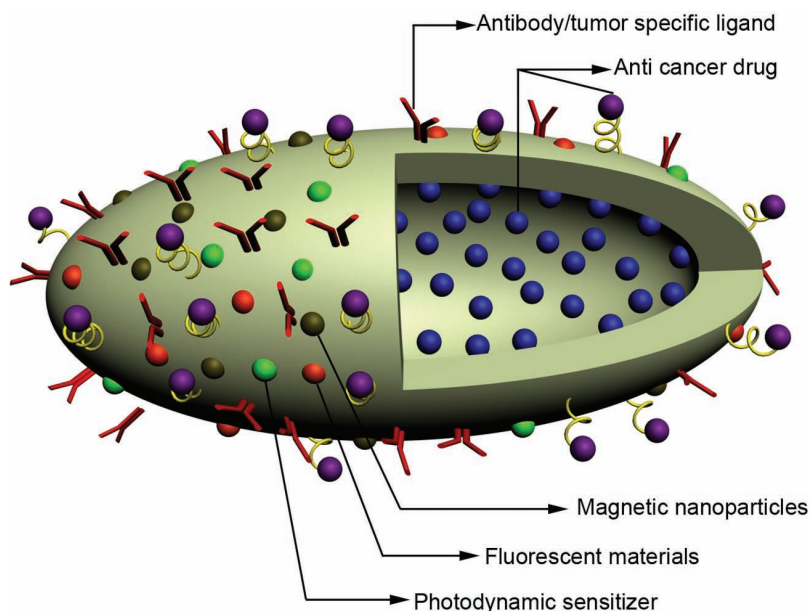


# Engineered Multifunctional Nanocarriers for Cancer Diagnosis and Therapeutics

Donglu Shi,\* Nicholas M. Bedford, and Hoon-Sung Cho



## From the Contents

1. Introduction .....	2550
2. In-Vivo Optical Imaging .....	2551
3. Drug Storage & Release .....	2553
4. Cell Targeting .....	2556
5. Cancer Treatment .....	2558
6. Outlook .....	2562

*This article reviews advances in the design and development of multifunctional carbon-based and/or magnetic nanoparticle systems (or simply ‘nanocarriers’) for early cancer diagnosis and spatially and temporally controlled therapy. The critical issues in cancer diagnosis and treatment are addressed based on novel nanotechnologies such as real-time in-vivo imaging, drug storage and release, and specific cancer-cell targeting. The implementation of nanocarriers into animal models and the subsequent effectiveness in treating tumors is also reviewed. Recommendations for future research are given.*

## 1. Introduction

Early detection of cancerous cells is critical to rapidly initiate treatment and consequently increase patient survival. The most common method used in cancer diagnosis is magnetic resonance imaging (MRI), which can readily detect lesions as small as a few millimeters.<sup>[1–6]</sup> Though the technique is applied as a major medical diagnostic tool, it is costly and time-consuming to implement. In clinical diagnosis, it can be difficult to achieve high spatial and temporal resolution simultaneously with MRI. In addition, significant nonspecific binding of MRI contrast agents can lead to difficulties in the interpretation of the diagnostic results which are largely dependent on the experience of the physician.<sup>[7]</sup> Such uncertainty in cancer diagnosis should be avoided if possible. While MRI is widely considered to be safe, some concerns were recently raised regarding the high magnetic fields produced by MRI instruments.<sup>[8–10]</sup> In comparative terms, optical imaging is much easier and cost-effective while providing rapid diagnosis with high resolution. For breast-cancer diagnosis, near-infrared optics has been combined with MRI as a potentially more accurate diagnostic methodology.<sup>[11]</sup> MRI produced the basic image of the breast while infrared imaging provided physiological information about the tissue, which could be used for the early detection of a developing cancer. Various advances in optical tomography techniques have also shown promise as inexpensive alternatives to MRI.<sup>[12–16]</sup>

The other aspect of this issue deals with cancer treatment, which is clinically a completely separate procedure. Severe side effects arise from the use of more classical cancer therapeutics due to nonspecificity of the cancer drug, resulting in high toxicity in noncancerous but rapidly dividing cells.<sup>[17–20]</sup> As such, more cancer-specific therapeutics are desired. A necessary aspect of cancer treatment can be surgery. Due to the lack of any bioluminescence, tumors can be difficult to locate and remove, particularly on the smaller size scales. This could lead to uncertainty in providing a conclusive assessment in surgery. Therefore, it is highly desirable to create a means by which cancer cells could be targeted with high specificity and be simultaneously imaged *in vivo*.

Due to the discovery of the enhanced permeability and retention effect,<sup>[21–23]</sup> nanotechnology-based treatments are aggressively being explored in an effort to improve the efficiency and accuracy of cancer diagnosis while providing highly specific, and highly efficient cancer therapeutics. Such multifunctional nanocarriers would ideally be porous for the loading of therapeutics and functionalized with both ligands, for cell specific targeting,<sup>[24–27]</sup> and fluorescent materials, for ease of detection. The nanocarrier can also be loaded with therapeutic moieties if desired. Furthermore, the loaded cancer drugs should be locally released in a controlled fashion by a defined stimulus in the environment (such as temperature, pH, biomarkers, or exposure to light).<sup>[28]</sup> The addition of a magnetic nanomaterial, such as nanocrystalline Fe<sub>3</sub>O<sub>4</sub>, would further extend the functionality of the nanocarrier. Localization of nanocarriers to tumors can be accomplished by using magnetic fields to concentrate the nanocarrier directly in tumors,<sup>[29–31]</sup> while magnetic hyperthermia<sup>[32–35]</sup> can be used to directly kill cancer cells<sup>[36–38]</sup> or

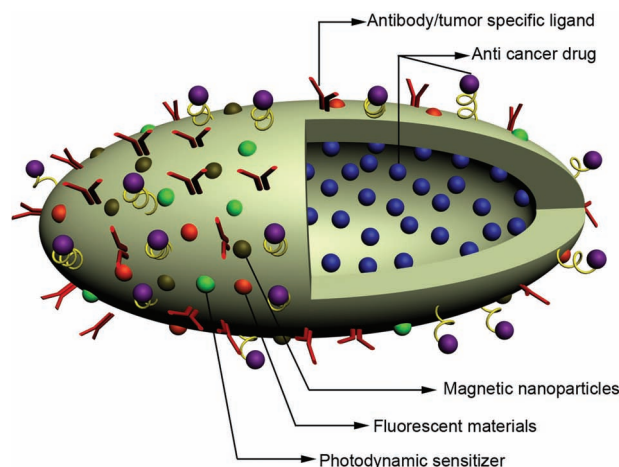


**Figure 1.** Schematic diagram illustrating an idealized nanocarrier system for cancer treatment and diagnosis. The average size of the nanocarriers should be 50–100 nm, depending on the specific biological process. Reproduced with permission.<sup>[7]</sup> Copyright Wiley-VCH, 2009.

as a trigger for controlled release.<sup>[39–44]</sup> A nanocarrier that was both highly luminescent and magnetic could also act as a bimodal imaging agent. For optimal fluid dynamical properties, an idealized 'football' shape has been proposed for this multifunctional nanocarrier, as seen in **Figure 1**.<sup>[7]</sup> The as-described multifunctional nanocarrier would be tumor-specific, allow for localized treatment, and be highly fluorescent which would allow for simultaneous diagnosis and treatment.

Carbon nanotubes (CNTs) are of particular interest as multifunctional nanocarriers for a cancer diagnosis and treatment as they exhibit many of the properties of the proposed multifunctional nanocarrier. CNTs are structurally anisotropic and hollow, which fulfill requirements for optimal fluid dynamics and for drug-storage properties, respectively. While not inherently biocompatible, fluorescent, or magnetic, the high thermal stability of CNTs allows for modification to the CNT's surface via chemical or physical processes.<sup>[45–48]</sup> The toxicity of CNTs is a controversial subject.<sup>[49]</sup> While there are conflicting reports in the literature, it is generally observed that longer CNTs pose a more serious health threat.<sup>[50]</sup> Furthermore, nonfunctionalized CNTs have appear to be more toxic<sup>[51–54]</sup> than nonfunctionalized

Prof. D. Shi  
The Institute for Advanced Materials and Nano Biomedicine  
Tongji University, Shanghai 200092, China

Prof. D. Shi, N. M. Bedford  
Department of Chemical and Materials Engineering  
University of Cincinnati, Cincinnati  
OH 45221, USA  
E-mail: shid@ucmail.uc.edu

Dr. H.-S. Cho  
Center for Translational Nuclear Medicine and Molecular Imaging  
Massachusetts General Hospital and Harvard Medical School  
Charlestown, Massachusetts 02129, USA

DOI: 10.1002/sml.201100436

CNTs.<sup>[55–59]</sup> Magnetic nanoparticles (MNPs) or magnetic nanospheres (MNSs) are also interesting candidates as substrates for multifunctional nanocarriers. A multifunctional MNS could be used for magnetic-based tumor targeting and tumor treatment as discussed above. Iron oxide nanomaterials are also moderately biocompatible and nontoxic.<sup>[60–63]</sup> A comparatively new class of nanomaterials, nanographene sheets (NGS) and nanographene oxide (NGO) have recently emerged as possible nanocarriers for cancer treatment. Graphene-based nanocarriers have an advantage over CNTs as graphene has twice the surface area of a CNT per carbon atom. Compared to CNTs, the available literature on graphene toxicity is quite small. Preliminary studies suggest that functionalized NGS<sup>[64]</sup> and NGO<sup>[65]</sup> are nontoxic, although more work is needed to better understand the cytotoxicity of graphene-based nanomaterials. The use of these three classes of nanomaterials as nanocarrier systems for cancer diagnosis and treatment will be the focus of this review. Other nanomaterial systems have been used as substrates for potential multifunctional nanocarriers, such as hydroxyapatite (HA) nanoparticles,<sup>[66,67]</sup> porous silica nanoparticles,<sup>[68,69]</sup> polymer micelles,<sup>[70,71]</sup> polymer nanoparticles,<sup>[72,73]</sup> lipid micelles,<sup>[74,75]</sup> dendrimers,<sup>[76,77]</sup> semiconductor quantum dots,<sup>[78–80]</sup> metallic nanoshells,<sup>[81,82]</sup> and metal–organic nanostructures.<sup>[83]</sup>

The format of this review will reflect the hierarchy of important functionalities needed to generate the ideal nanocarrier for cancer diagnosis and treatment. First the functionalization of CNTs, MNP/MNSs, and NGS/NGOs with highly luminescent materials for in-vivo optical imaging will be discussed. This will be followed by drug-loading techniques onto such nanocarriers and the subsequent controlled release of therapeutic agents. From there, functionalization of specific targeting moieties on such nanocarriers will be reviewed for in-vitro targeting. Combining any number of the aforementioned requirements would yield a potential nanocarrier system. Testing such nanocarrier systems in vivo will be reviewed last. The end of the review will include comments on the future of the field.

## 2. In-Vivo Optical Imaging

For successful in-vivo imaging (especially deep-tissue imaging), the fluorescent moiety needs to brightly emit in the IR as most biological materials do not absorb in this wavelength region.<sup>[84]</sup> CNTs exhibit weak IR fluorescence,<sup>[85]</sup> and therefore need to be functionalized with a highly IR fluorescent material for deep tissue imaging. Semiconductor quantum dots (QDs) have been of interest for in-vivo imaging largely due to their intense fluorescence emissions. The size-tunable optical properties seen in QDs allow for the synthesis of highly IR-emitting nanomaterials. In addition, QDs exhibit high quantum yields, sharp emission spectra, and a high resistance to photo-bleaching.<sup>[86–90]</sup>

Whole-body in-vivo imaging of mice was accomplished using QD-conjugated multiwall carbon nanotubes (MWCNTs) as reported by Shi et al.<sup>[91]</sup> MWCNTs were functionalized with carboxylic acid groups to allow for QD



**Donglu Shi** received his PhD in Engineering in 1986 from the University of Massachusetts. After graduation, he took a Staff Scientist position at the Materials Science Division of Argonne National Laboratory in 1987. In 1995, Donglu Shi joined the faculty in the Department of Materials Science and Engineering at University of Cincinnati. Donglu Shi has so far published more than 200 refereed journal publications and is currently the Editor-in-Chief of *Nano LIFE*, and Associate Editor of *Materials Science & Engineering: C* and *Journal of Nanomaterials*. Donglu

Shi's main interests include nanostructured materials and nano-biomedicine. His most recent works on nano-biomedicine pioneer a novel approach in the assembly of intelligent nanosystems for early cancer diagnosis and localized treatment.



**Nicholas M. Bedford** received a Bachelor degree in both chemistry and physics from Central Michigan University in 2007. He is currently a PhD candidate at the University of Cincinnati in the department of Materials Science and Engineering under the supervision of Dr. Donglu Shi and Dr. Andrew Steckl. He also spends time working at the Air Force Research Laboratory in the research group led by Dr. Rajesh Naik. His main research interests include electrospinning of functional materials, nano–bio interfaces, nano-biomedicine, and conjugated polymers.



**Hoonsung Cho** is a Post Doctoral Research Fellow in the Center for Translational Nuclear Medicine and Molecular Imaging at the Massachusetts General Hospital. He received his doctoral degree from the University of Cincinnati in 2010 under the supervision of Prof. Donglu Shi, with a major focus on the development of a multifunctional nanocarrier system for imaging, drug delivery, and cell targeting in cancer research. His current research interests include imaging cell death with multimodal vital fluorochromes.

conjugation. This was accomplished using a plasma polymerization process to deposit acrylic acid (AA) previously developed by the group.<sup>[92,93]</sup> A uniform 2 nm-thin film was deposited on the MWCNTs using this method, which was shown using transmission electron microscopy (TEM). The amine-functionalized QDs were covalently immobilized on carboxylic acid-functionalized MWCNTs via standard coupling techniques. Bright-field TEM images of the MWCNT–QDs are shown in **Figure 2**. In this example, CdSe/ZnS core/shell QDs were used. The QDs appear darker in contrast in the TEM and are randomly distributed along the MWCNTs (Figure 2a). High-resolution TEM (HRTEM) images clearly show nanocrystalline QDs on the surface of the AA-functionalized MWCNT (Figure 2b,c). The accompanying electron diffraction pattern is a result of the diffuse diffraction signature of the (002) graphite layer in the MWCNTs, and ring patterns from the CdSe/ZnS QDs (inset, Figure 2b). These materials were also characterized using energy dispersive X-ray

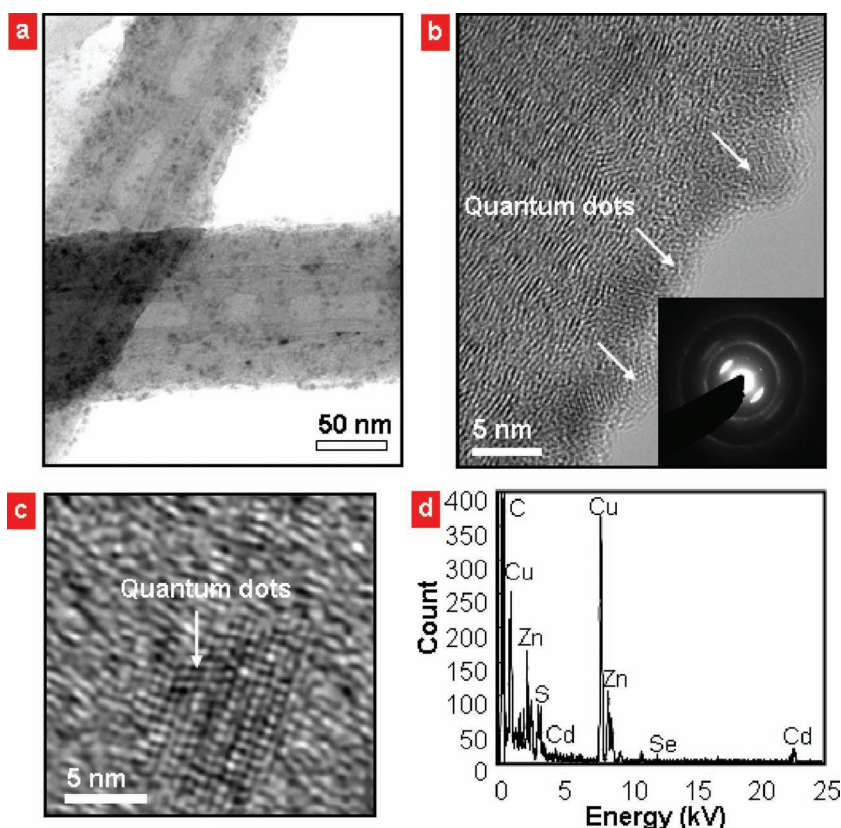


**Figure 2.** a) Bright-field TEM image of QD-coupled MWCNTs; b,c) HRTEMs showing the crystal structure of the CdSe/ZnS QDs (inset in (b) is the corresponding electron diffraction pattern); d) EDS spectrum from the QD-functionalized MWCNTs. Reproduced with permission.<sup>[91]</sup> Copyright Wiley-VCH, 2007.

spectroscopy (EDS) to further confirm the presence of the QDs (Figure 2d). The room temperature luminescence spectrum of MWCNT-QDs was shown to have a maximum around 610 nm, which is redshifted from the original QD spectrum of 600 nm. This spectrum shows that that QD fluorescence is not quenched by the MWCNT, an important requisite for in-vivo imaging.

Fluorescent MWCNTs using CdSe/ZnS QDs and InGaP/ZnS QDs (610 and 680 nm maximum emission wavelengths, respectively) were then used for in-vivo imaging in mice (Figure 3). Mice were injected with 10  $\mu\text{L}$  of the MWCNT-QD suspension at various locations from head to tail and at different MWCNT-QD concentrations. Figure 3a shows an in-vivo image of a mouse injected at a middorsal location with CdSe/ZnS QDs. For CdSe/ZnS QDs, it was found that concentrations above 0.125  $\mu\text{g mL}^{-1}$  exhibit highly pronounced luminescence (Figure 3b, locations A, B and C), while concentrations as low as 0.0625  $\mu\text{g mL}^{-1}$  could still be seen (Figure 3b, location E). In-vivo imaging with InGaP/ZnS-based MWCNT-QDs yielded images with much brighter fluorescence than the CdSe/ZnS-based material (Figure 3c). This is attributed to a decrease in background absorption from the mouse as the emission wavelength of the QD is longer. Nanocarriers with emission wavelengths between 700 and 800 nm would be more ideal for in-vivo imaging and are used in later studies reviewed in this paper. Nevertheless, these MWCNT-QDs first reported

by Shi et al. show that MWCNTs could be used as a platform for in-vivo imaging and eventual cancer treatment.

Using a similar strategy, MNS can be functionalized with QDs.<sup>[94]</sup> MNSs are of interest as they can potentially allow for cancer treatment via magnetic hyperthermia. Magnetic hyperthermia is a heating phenomenon caused by magnetic nanoparticles when subjected to an alternating magnetic field.<sup>[7]</sup> In order for the MNSs to be used in the cancer treatment applications, they have to show superparamagnetic properties under zero magnetic field. Typically,  $\text{Fe}_3\text{O}_4$  shows ferromagnetic properties. However, superparamagnetic properties can be obtained if the nanoparticles are below  $\approx 10$  nm and monodispersed.<sup>[95-97]</sup> A consequence of synthesizing MNPs on this size scale is a significantly reduced magnetic moment for each particle. MNSs overcome this shortcoming by coupling several  $\text{Fe}_3\text{O}_4$  nanoparticle within a larger polymeric nanoparticle, thus retaining both high magnetic moments and superparamagnetic properties.

Shi et al.<sup>[94]</sup> created such MNS-QD conjugates via the schematic shown in Figure 4. Using a miniemulsion/emulsion polymerization technique,<sup>[98]</sup> polyethylene glycol (PEG)-modified polystyrene-iron oxide ( $\text{PS-Fe}_3\text{O}_4$ ) MNSs were synthesized.

Through the auto-oxidation of surface PEO, amine-functionalized QDs were coupled to MNSs by conventional carbodiimide chemistry. MNSs conjugated with CdSeTe/ZnS were found to be  $\approx 100$  nm in diameter, which is suitable for medical applications.<sup>[99]</sup> Images from TEM show darker contrast 5–10 nm particles within a lighter contrast spherical structure, which corresponds to the  $\text{Fe}_3\text{O}_4$  nanoparticles and PS nanoparticle respectively (Figure 5a). An HRTEM image of the periphery of the MNS-QD shows regions of ordered lattice structures, which can be indexed to ZnS in the QDs (Figure 5b). The fluorescence of these QD-MNSs is shown in Figure 6, with a maximum emission wavelength of 770 nm. This emission is blueshifted from the original QDs. The nanocarriers presented here could potentially be used as bimodal imaging agents while treating the tumor region using magnetic hyperthermia.

Combining a stable template (CNT), a highly fluorescent material (QD), and a magnetic moiety ( $\text{Fe}_3\text{O}_4$ ) into one signal nanocarrier would be of great medical interest as it would allow for optical diagnosis and treatment via magnetic hyperthermia. To this end, QDs and  $\text{Fe}_3\text{O}_4$  were attached to MWCNTs as reported by Shi et al.<sup>[100]</sup> Plasma polymerization was used to surface-functionalize MWCNTs with poly(lactic-co-glycolic acid) (PLGA). PLGA is biodegradable and Food and Drug Administration-approved for use as a polymeric drug-delivery system. Amine-functionalized

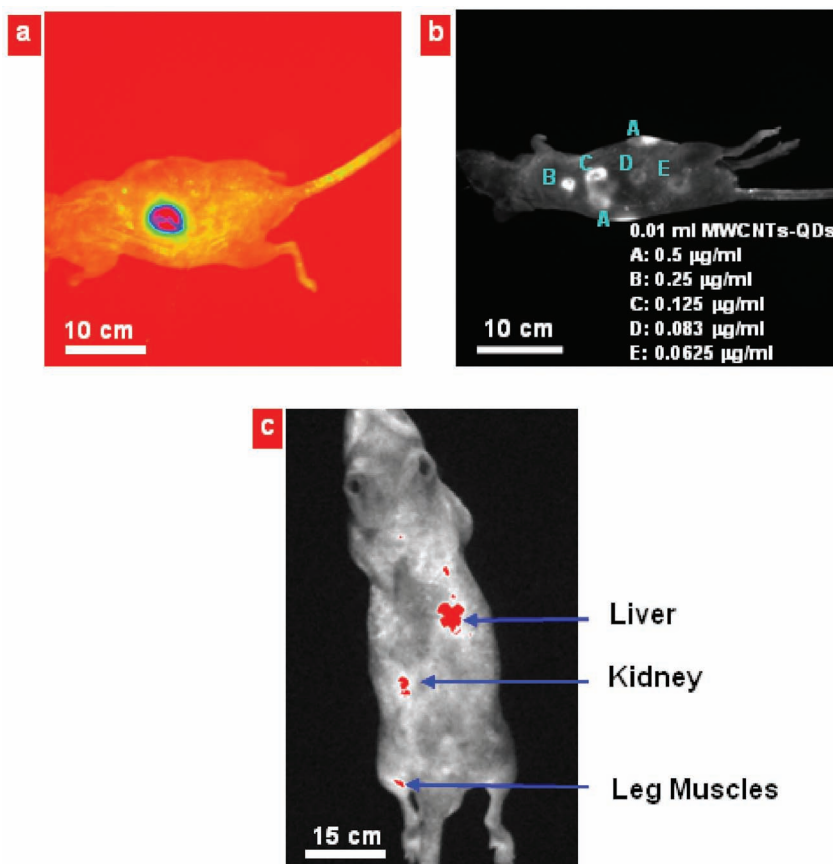


**Figure 3.** In-vivo images of MWCNT-QDs in mice injected at different body regions: a) CdSe/ZnS-based MWCNT-QDs (emission at 600 nm) at middorsal location, b) the same nanocarrier system as in (a) at ventrolateral locations (concentration of nanocarriers given in A through E), and c) InGaP/ZnS-based MWCNT-QDs (emission at 680 nm) in liver, kidney, and leg muscles. All images were taken in 2 min under epi-UV illumination with an excitation wavelength of 435 nm. Reproduced with permission.<sup>[91]</sup> Copyright Wiley-VCH, 2007.

QDs and  $\text{Fe}_3\text{O}_4$  nanoparticles were attached to the surface of the functionalized MWCNTs. The nanocarrier exhibits a blueshift of 20 nm from the original 800 nm peak emission of the free QDs. This was attributed to interactions between the QDs and CNTs, as discovered in a previous study.<sup>[101]</sup> The magnetic hysteresis curve and magnetic hyperthermia curve for CNT-QD- $\text{Fe}_3\text{O}_4$  and CNT- $\text{Fe}_3\text{O}_4$  are shown in **Figure 7a,b**. The nanocarrier shows a typical magnetic

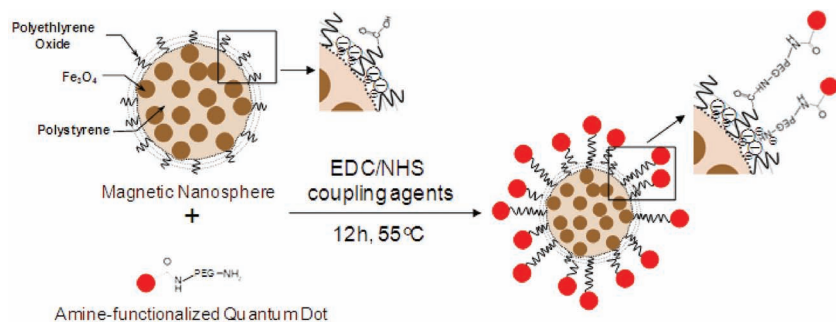


**Figure 4.** Schematic of MNS-QD coupling. EDC: 1-ethyl-3-(3-dimethylaminopropyl) carbodiimide HCl, NHS: *N*-hydroxysuccinimide, PEG: poly(ethylene glycol). Reproduced with permission.<sup>[94]</sup> Copyright Wiley-VCH, 2009.

hysteresis, with a small amount of irreversibility. The hyperthermia curves are similar for the two CNT- $\text{Fe}_3\text{O}_4$  tests, and produce a temperature of 45 °C after 30 min using a 956 kHz, 6.0 mT magnet field. This set of testing conditions and temperature ranges is preferable for cancer treatment, while potentially allowing in-vivo imaging. In-vitro and in-vivo imaging and magnetic hyperthermia were not reported, although this nanocarrier system could serve as a potential starting point for such experimentation.

The previous studies illustrate the possibility of using CNTs and MNSs as multifunctional nanocarriers and can be used as a starting point for further functionality in diagnosis and cancer treatment. Fluorescent MNSs could also serve as bimodal imaging agents. While QD- $\text{Fe}_3\text{O}_4$  was reviewed here, magnetic nanoparticles could also be functionalized with conjugated polymers<sup>[102]</sup> and plasmonic materials<sup>[103,104]</sup> for bimodal imaging as well. These highly fluorescent nanostructures can be conjugated to the biocompatible nanocarriers for in-vivo imaging, which can be useful for easier cancer diagnosis. The following sections of the review will highlight strategies for drug storage and release, specific targeting, and cancer treatment using similar multifunctional nanocarrier templates.

### 3. Drug Storage & Release

The ability to locally deliver drugs to tumor cells concentrated only in cancerous regions of the body is a key challenge in cancer therapeutics. The more commonly used cancer drugs broadly distribute throughout the body and negatively impact on the proliferation of noncancerous cells. Nanocarrier systems could circumvent these issues by providing an environment for drug storage by increasing the dose unit per volume while controlling the rate of release by engineering specific functionalities into the nanocarrier. In this way, anticancer drugs can be used much more efficiently, which in turn would lower the total amount of drug administered. Key challenges in this area include the prevention of drug leakage during biodistribution and effectively releasing the drug at the point of contact with cancer cells. In the following section, key studies will be reviewed that take aim at such challenges.

Using MWCNTs as nanocarriers, Guo et al.<sup>[105]</sup> examined drug storage and

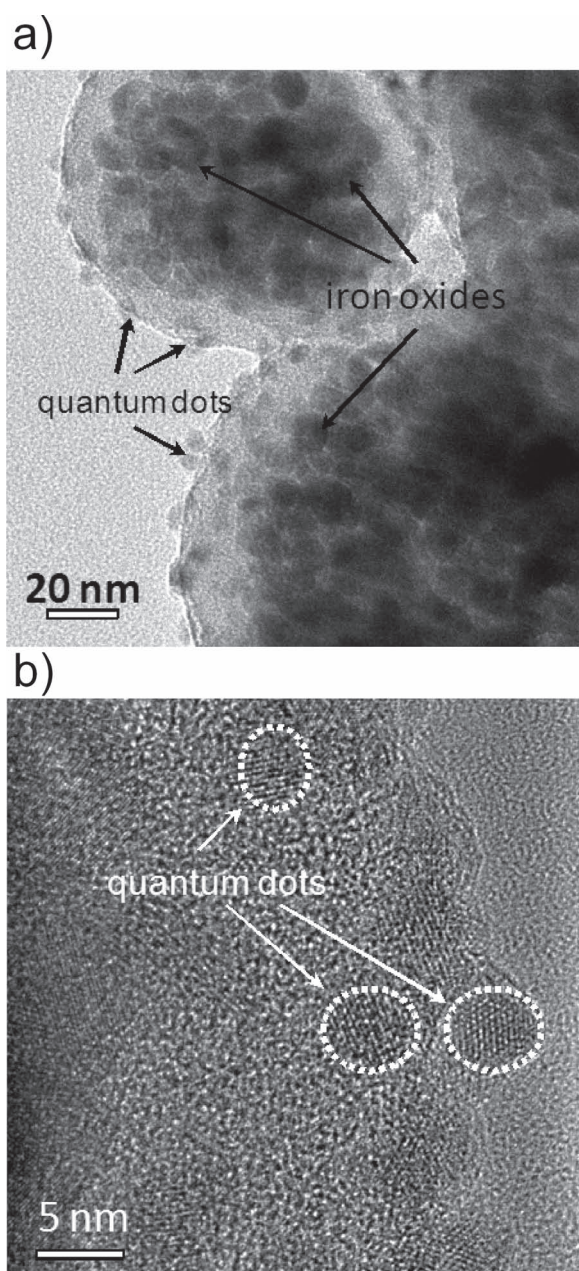


Figure 5. a) Bright-field TEM images of MNS-QDs, and b) an HRTEM image showing the lattice structure of the QDs. Reproduced with permission.<sup>[7]</sup> Copyright Wiley-VCH, 2009.

cancer cell treatment in vitro. MWCNTs were first functionalized with PLGA via plasma polymerization. Paclitaxel (PTX), an antitumor agent used in the clinic for a variety of tumors,<sup>[106,107]</sup> is used as a model drug in this study. Drug loading was done by simply mixing PLGA-coated MWCNTs in a methanolic drug solution, followed by solvent evaporation and repeated washing with distilled water. The amount of PTX loaded onto/into the MWCNTs was found to be  $113 \pm 6 \mu\text{g mg}^{-1}$  CNT, as determined by HPLC.

PTX-loaded MWCNTs were tested against human PC-3MM2 prostate cancer cells using a (3-(4,5-dimethylthiazol-2-yl)-2,5-diphenyltetrazolium bromide (MTT) assay (Figure 8). Cell viability was tested after a 96 h incubation

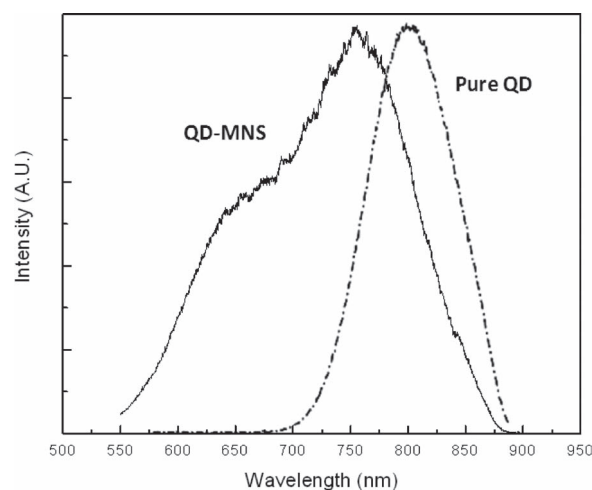


Figure 6. Emission spectra of pure QDs and MNS-QDs. Reproduced with permission.<sup>[7]</sup> Copyright Wiley-VCH, 2009.

period. A PTX concentration of  $5 \text{ ng mL}^{-1}$  was found to be sufficient to kill  $\approx 50\%$  of the prostate cancer cells. PTX-loaded MWCNTs showed a similar level of cell death at a concentration of  $100 \text{ ng mL}^{-1}$ . The author's predicted that a dosage of  $0.5 \text{ ng}$  paclitaxel was released from the PLGA coating, which corresponds to  $\approx 50\%$  of the loaded antitumor drug (based on

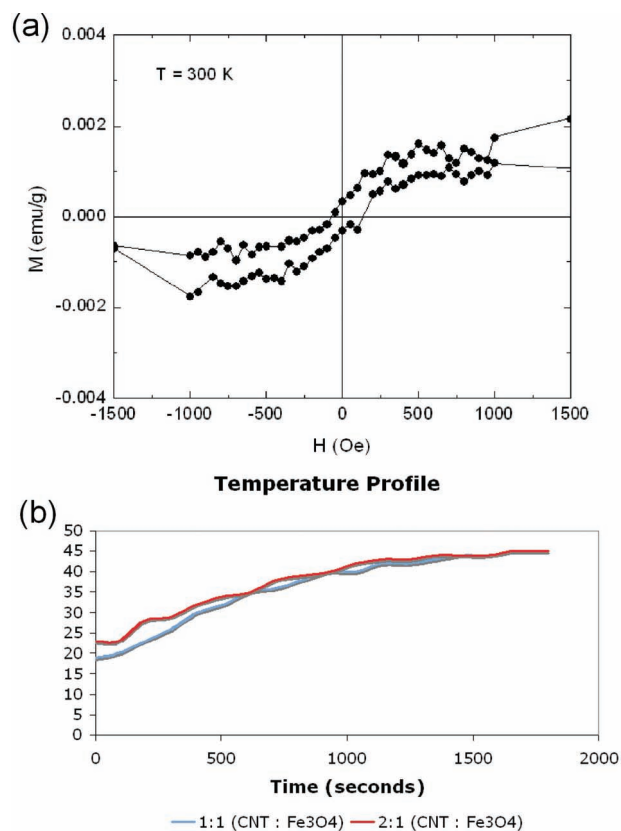
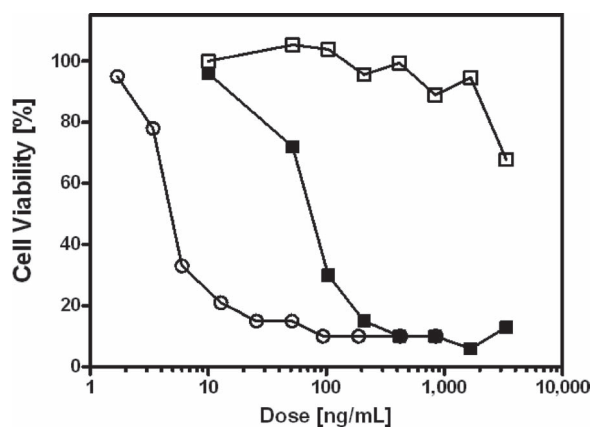


Figure 7. a) Room-temperature magnetization versus applied field for QD- $\text{Fe}_3\text{O}_4$ -CNT, and b) hyperthermia temperature-versus-time curves for nanocarriers at different CNT: $\text{Fe}_3\text{O}_4$  ratios. Reproduced with permission.<sup>[100]</sup> Copyright American Institute of Physics, 2009.



**Figure 8.** Dose-dependent effects on CNTs and PTX on the viability of human PC-3MM2 prostate cancer cells in vitro over a 96 h period. Hollow spheres represent free PTX, solid squares represent PTX-loaded, PLGA-coated CNTs, and the hollow squares represent PLGA-coated CNTs without PTX. Reproduced with permission.<sup>[105]</sup> Copyright Wiley-VCH, 2008.

the positive control and HPLC data). The drug-free PLGA-coated MWCNTs did not show any sufficient cellular death until concentrations exceeding 1000 ng mL<sup>-1</sup>. It is worth noting that issues could arise with noncontrolled release, as PLGA is a biodegradable polymer. Regardless, the data shows that drug-loaded PLGA-coated MWCNTs kill prostate cancer cells at a higher dose-per-unit-volume than free PTX. These nanocarrier systems have an increased water solubility compared to this lipophilic antitumor agent, and have the added benefit of being a nanocarrier platform that could undergo further functionalization for improved cancer treatments strategies (i.e., magnetic functionalization for hyperthermia, ligands for specific targeting, etc.).

Drug-loaded, self-assembled poly(vinyl alcohol)-iron oxide/silica core/shell (SAIO@SiO<sub>2</sub>) MNSs were successfully synthesized and tested for drug release using a high-frequency magnetic field (HFMF) by Hu et al.<sup>[108]</sup> Using magnetic hyperthermia, the drugs would be released from the MNSs due to the increased polymer-chain mobility at higher temperatures. The motivation behind using a thin shell of silica was to regulate unintentional drug release. The size regimes for the nanoparticles synthesized here were 4.8, 76.7, and 85.6 nm for Fe<sub>3</sub>O<sub>4</sub>, SAIO, and SAIO@SiO<sub>2</sub> nanoparticles, respectively. Using ibuprofen (IBU) as a model hydrophobic drug, it was shown that uncapped SAIO would release a large majority of the drug over a 1 h period, while SAIO@SiO<sub>2</sub> nanoparticles exhibited a comparatively very small release of IBU over the same time period. Under HFMF, the SAIO nanoparticles would exhibit slow-to-burst release profiles for all HFMF times tested, which increased linearly with stimulus time (Figure 9a). Upon removal of the HFMF, the SAIO nanoparticles maintained burstlike release profiles, and the release rate was increased when compared to SAIO nanoparticles without HFMF treatment. The SAIO@SiO<sub>2</sub> nanoparticles exhibit similar slow-to-burst release profile after HFMF treatment, albeit with two important differences. The overall release of IBU was decreased by approximately two-fold when compared to SAIO nanoparticles and, upon

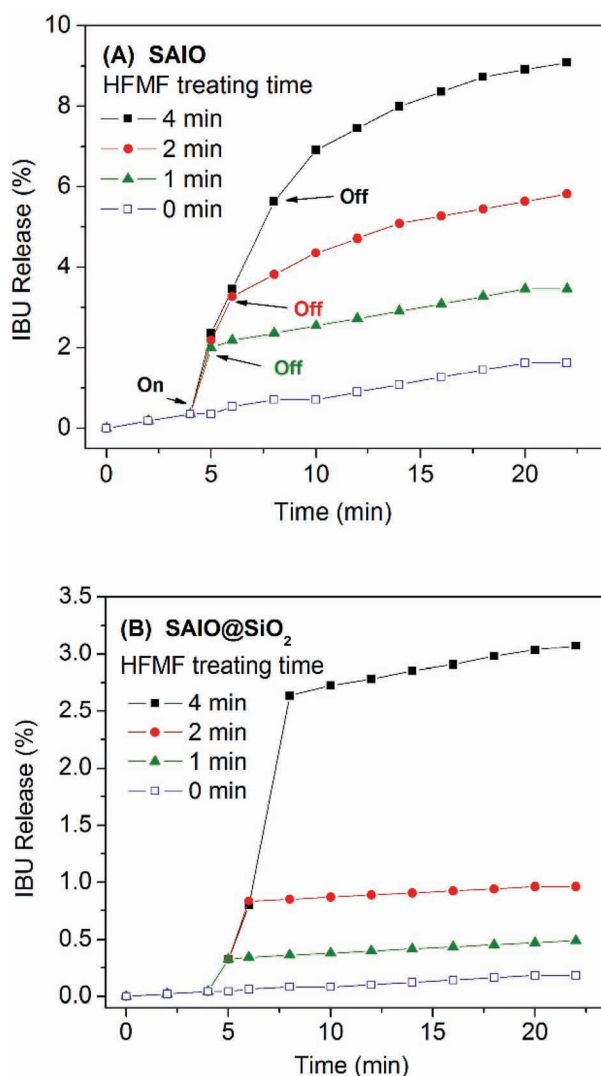


**Figure 9.** a) Drug-release profiles for SAIO and SAIO@SiO<sub>2</sub> nanocarriers under no HFMF; b) drug-release profiles for SAIO under HFMF treatment for 1–4 min, and; c) drug-release profiles for SAIO@SiO<sub>2</sub> under HFMF treatment for 1–4 min. Reproduced with permission.<sup>[108]</sup> Copyright Wiley-VCH, 2008.

removal of the HFMF, the zero-order release profile was recovered (Figure 9b). The authors attributed both of these distinct differences to the silica shell's ability to regulate IBU diffusion out of the nanoparticles.

The cellular uptake of SAIO@SiO<sub>2</sub> nanoparticles was studied in HeLa cells using fluorescein isothiocyanate (FITC)-labeled nanocarriers and photoluminescence microscopy. It was found that SAIO@SiO<sub>2</sub> nanoparticles were gradually internalized by HeLa cells over a 4 h period, which was attributed to endocytosis. Similar uptake results were seen using flow cytometry as well. The SAIO and SAIO@SiO<sub>2</sub> nanoparticles were also shown to be nontoxic using MTT assay. The two nanocarriers were tested over a 48 h period, with almost no loss in cell viability. Magnetically induced drug release from the nanocarrier in HeLa cells was not shown in this study, nor was a more relevant cancer therapeutic tested. However, this system shows promise for cancer therapeutics,

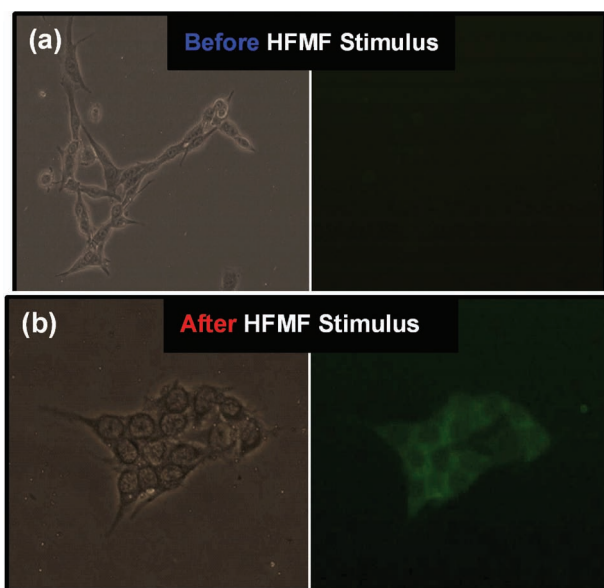


**Figure 10.** Fluorescence microscopy images of HeLa cells after 10 h incubation with fluorescence-loaded, PVP-modified  $\text{SiO}_2/\text{Fe}_3\text{O}_4$  MNSs without HFMF treatment (a) and 30 s of HFMF treatment (b). Reproduced with permission.<sup>[109]</sup> Copyright Wiley-VCH, 2008.

as the potential to magnetically localize and trigger a controlled release of an anticancer drug is desirable to efficiently treat tumors.

The same group also developed a similar MNS system wherein a core phase of poly(vinyl pyrrolidone) (PVP)-modified silica with fluorescent dye (used as a drug model) is capped with a  $\text{Fe}_3\text{O}_4$  shell.<sup>[109]</sup> The HFMF was shown to induce nanoscale faults within the  $\text{Fe}_3\text{O}_4$  shell, which allow for the release of the fluorescence molecules. These MNSs were shown to enter HeLa cells. A HFMF was applied to the HeLa cells and green fluorescence was observed throughout the HeLa cells (**Figure 10**). In a follow-up study,<sup>[110]</sup> the nanocrystalline Zn–Cu–In–S (ZCIS) QDs were grown on the surface of the MNSs. While immobilization of QDs on the surface of the MNSs could potentially allow optical diagnosis of cancer cells, they also serve a secondary purpose: as a HFMF is applied, thermal energy from the  $\text{Fe}_3\text{O}_4$  is used to effectively quench the QDs via exciton dissociation between QDs.<sup>[110]</sup> Upon exposure to a HFMF, the fluorescence intensity of the QDs decreased with an increased exposure time, while the fluorescence from the model drug consequently increased. This suggests that the amount of drug released could possibly be quantified by measuring the decreased fluorescence from the QDs, as both events are a consequence of the applied magnetic field. The changes in intensity of both the drug model and QDs changed linearly at varying magnetic field strengths, indicating that quantification of drug release could be possible. This effect was also confirmed in vitro with HeLa cells.

Employing rare earth (RE) doped phosphates over QDs, Wang et al.<sup>[111]</sup> synthesized MNSs loaded with the anticancer drug doxorubicin (DOX). While generally not as luminescent as QDs, RE-based materials are less toxic than the more common variants of QDs, which is an important requisite

for a clinically viable nanocarrier.  $\text{YPO}_4$  particles doped with either Eu or Tb were synthesized by a solvothermal technique and then coprecipitated with  $\text{Fe}^{3+}$  and  $\text{Fe}^{2+}$  to form  $\text{Fe}_3\text{O}_4$ . DOX was loaded onto the MNSs in PBS buffer at a DOX-encapsulation efficiency of 69.6% and DOX-loading content of 18.7%. DOX shows a 17.3% release from Tb-based MNSs after 6 h, followed by a slow release of the drug for up to five days, beyond which the release profile plateaus out just below 25% of the initial loaded DOX amount. These MNSs were found to successfully accumulate in HeLa cells after a 96 h incubation period. No in-vitro release of DOX in cancerous cells was reported, nor was there any report of magnetically induced drug release.

PEG-functionalized NGOs were used as a carrier for anticancer drugs as reported by Liu et al.<sup>[112]</sup> SN38, an aromatic topoisomerase I inhibitor,<sup>[113]</sup> was chosen because of its potent anticancer properties and poor water solubility. SN38 is derived from the clinically relevant CPT-11 via a metabolic reaction in the body, but much of the original CPT-11 is excreted prior to SN38 formation or metabolized into other, inactive compounds.<sup>[114]</sup> SN38 was believed to bind to the water-soluble PEG–NGO via hydrophobic interactions and  $\pi$ – $\pi$  stacking between the aromatic regions of the drug and NGO. Fluorescence quenching of SN38 on the NGO and the drug's zero-release profile in PBS buffer illustrated the high affinity of SN38 to NGO. The drug-loaded PEG–NGO was tested for cancer cell killing capability against the human colon cancer cell line HCT-116. Water-soluble CPT-11 exhibited a 50% decrease in cell viability at  $\approx 10 \mu\text{M}$ , while SN38-loaded nanocarriers exhibited similar cell killing at  $\approx 6 \text{ nM}$ , an impressive 1000-fold improvement (**Figure 11a**). The nanocarrier exhibited similar cell killing capabilities as free SN38 in DMSO. The PEG–NGOs without the loaded drug were found to be nontoxic, indicating that apoptosis was only caused by SN38 (**Figure 11b**). This data illustrates the potential for using graphene nanocarriers as an efficient drug-delivery agent for aromatic, insoluble drugs.

The preceding studies in this section highlight the ability to successfully incorporate commonly used cancer drugs or drug models into carbon-based and magnetically viable nanocarriers. It was shown that carrier-associated drugs are efficient at killing cancer cells in vitro, while the use of a magnetically active nanocarrier allows for a means to trigger the release of cancer therapeutics. Such characteristics are desired for smartly designed nanocarrier systems. To be used advantageously in medical environments, these nanocarriers would need specific targeting functionalities while also being tested in vivo, as reviewed in the subsequent sections.

#### 4. Cell Targeting

In order to reduce the toxic side effects of cancer treatment due to the nonspecific pharmacological uptake of cancer therapeutics by noncancerous cells, specific targeting strategies should be implemented. In a nanocarrier system, such specificity could be obtained by functionalizing the nanocarrier with a binding moiety (such as an antibody) that interacts with a biomarker specifically expressed on the

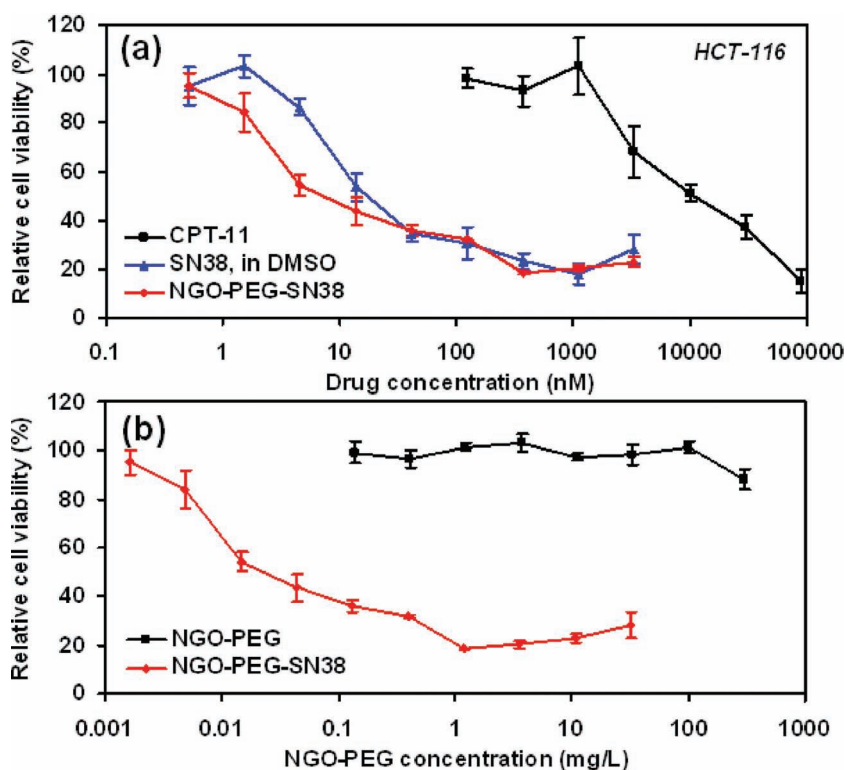


**Figure 11.** In-vitro cell toxicity assay of HCT-116 cells. a) Cell-viability data against CPT-11 in PBS, SN38 in DMSO, and NGO-PEG-SN38 in PBS at different concentrations over 72 h, and b) cell-viability data of nanocarriers with (red) and without (black) loaded SN38. Reproduced with permission.<sup>[112]</sup> Copyright ACS, 2008.

surface of a cancer cell. Combining cell-targeting strategies with the drug-loading and -release strategies reviewed in the previous section, would further enhance the efficiency of a nanocarrier system to effectively kill cancer cells. This section will highlight reports on specific cell-targeting strategies in vitro.

Specific targeting of cancerous cells using CNTs was reported by Kam et al.<sup>[115]</sup> Single-walled carbon nanotubes (SWCNTs) were functionalized with a phospholipid-polyethyleneglycol-amine (PL-PEG-NH<sub>2</sub>) and bound to folic acid (FA) through conventional coupling chemistry. The folic acid functionality is used to specifically bind to folate receptors (FR) that are typically overexpressed in cancer cells.<sup>[116]</sup> Using IR light to locally heat FA-SWCNTs, cells exhibiting FRs were specifically targeted and killed in vitro. Cells not expressing FR showed no cell death during the IR exposure and little SWCNT uptake when compared with FR-positive cells. In a similar study by Shao et al.,<sup>[117]</sup> SWCNTs were functionalized with antibodies for insulinlike growth factor 1 receptor (IGF1R) and human endothelial receptor 2 (HER2/neu). These receptors are found to be overexpressed in a variety of cancer cells as compared to healthy cells. IR laser pulses were used to effectively kill cancer cells that had expressed the receptor complementary to the targeting ligand on the SWCNT, while nonfunctionalized SWCNTs only killed 20% of cells. The use of IR light for phototherapy in these studies is advantageous as biological tissues and liquids do not absorb this wavelength of light. IR-basZed

phototherapy techniques such as these should be exploited further in future studies, as it is a moderately easy method for treating cancer cells.

Welsher et al.<sup>[118]</sup> have also reported antibody functionalization of SWCNTs. The antibody Rituxan was used to selectively bind CD20 (present on the surface of B-cells, but not T-cells) while Herceptin was used to selectively recognize HER2/neu. The HER2/neu receptor is found to be overexpressed in breast cancers.<sup>[119–121]</sup> The authors of this study emphasized the potential use of the SWCNT as a IR-fluorescent material that could be used for cancer diagnosis. Targeting studies on the Herceptin-functionalized SWCNTs with the HER2/neu positive BT-474 cell line and the MCF-7 cell line as the negative control are shown in **Figure 12**. The antibody-specific SWCNTs were bound to the BT-474 cell line and not to the MCF-7 in vitro, as expected. While CNTs alone may not suffice as a fluorescent material for deeper tissue in-vivo imaging, the aforementioned study was the first to show that properly functionalized CNTs could be used for specific cancer cell bioimaging. Further modification of these nanocarriers with IR-emitting materials would yield more promising in-vivo images.

Zhang et al.<sup>[122]</sup> used FA-functionalized SWCNTs loaded with DOX for targeted and controlled cancer treatment in

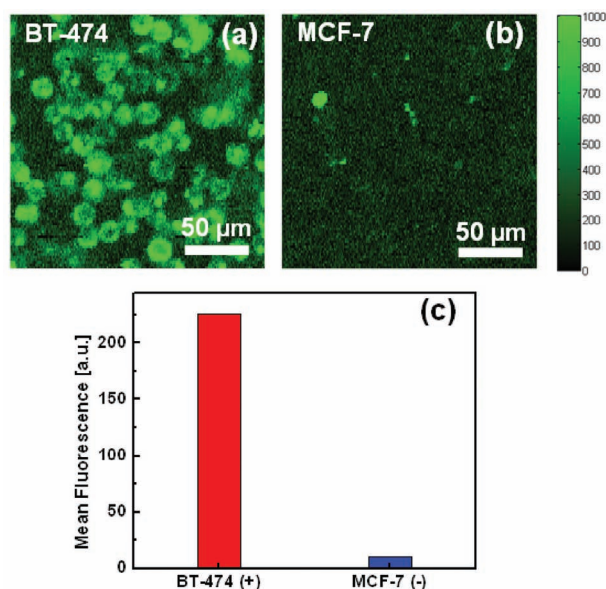


**Figure 12.** a) IR fluorescence image of BT-474 cells (HER2/neu positive) treated with SWCNT-Herceptin; b) IR fluorescence image of MCF-7 cells (HER2/neu negative) treated with SWCNT-Herceptin, and; c) average IR fluorescence values of (a) and (b) with a positive/negative ratio of about 20:1. Reproduced with permission.<sup>[118]</sup> Copyright ACS, 2008.

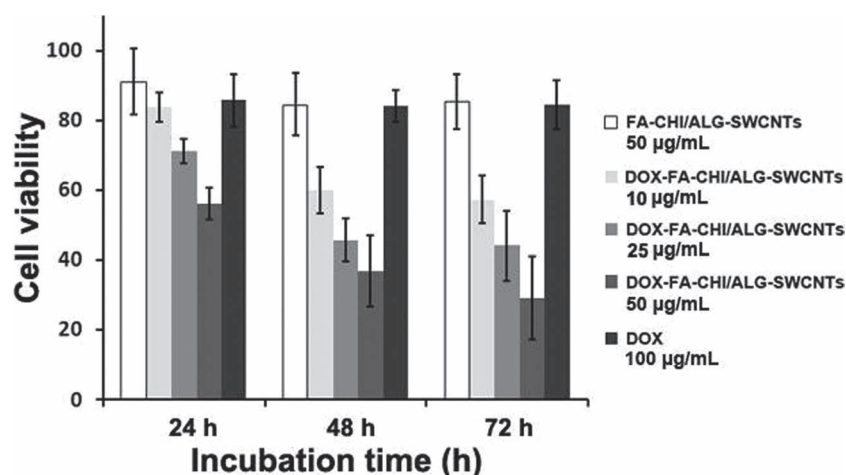


**Figure 13.** Cell viability of HeLa cells treated with various nanocarriers at different concentrations and incubation times. Reproduced with permission.<sup>[122]</sup> Copyright Elsevier, 2009.

vitro. The SWCNTs were coated with sodium alginate (ALG) and/or chitosan (CHI) to improve biocompatibility, followed by the coupling of FA and loading of DOX. It was found that ALG-SWCNTs loaded DOX more efficiently than CHI-SWCNTs, while the rate of release at lysosomal pH was found to be faster for CHI-SWCNTs than ALG-SWCNTs. CHI/ALG-SWCNTs exhibit immediate DOX-loading efficiency and rate-of-release comparable to the single polysaccharide coating. All nanocarrier systems tested showed little release at physiological pH (7.4). This is an advantageous property of these systems, as release of DOX could be triggered after entering the lysosome of a targeted cancer cell (pH = 5.8). The mechanism behind DOX release was not alluded to in this study. As with the previously referenced studies, these CNT-based nanocarriers were only specific to HeLa cells expressing FR and not to other cells. HeLa cell viability was tested against varying concentrations of FA-CHI/ALG-SWCNTs (**Figure 13**). The response to the DOX-loaded SWCNTs was found to be linear with dosage. More notable is that the nanocarriers killed more cells than did a higher concentration of unbound DOX. This study also highlights a more subtle strategy for drug loading and release, which is to employ two different materials to better optimize the loading and release kinetics of the cancer drug.

Magnetic nanomaterials surface-functionalized with target-specific ligands have been used for MRI applications for quite some time.<sup>[123–127]</sup> Huh et al.<sup>[128]</sup> were the first to demonstrate the use of cell-specific targeting and fluorescence detection using appropriately functionalized magnetic nanoparticles. While the bulk of this study was focused on MRI applications, the use of a FITC-tagged secondary antibody along with Herceptin allowed for specific optical detection of breast-cancer cells in vitro. Das et al.<sup>[129]</sup> made a similar MNS system using rhodamine isothiocyanate (RITC) as a fluorescent marker and FA as a targeting ligand for HeLa cells. In these two studies, IR-emitting materials would be needed for practical in-vivo imaging. Lee et al.<sup>[130]</sup> created MNSs by loading 12 nm Fe<sub>3</sub>O<sub>4</sub> nanoparticles into 100 nm glycol

chitosan nanoparticles. The MNSs were also functionalized with *N*-acetyl histidine for hydrophobic interactions, bombesin for targeting gastric-releasing peptide receptors overexpressed in prostate-cancer cells, and Cy5.5 for infrared optical detection. MNSs functionalized with bombesin were found to bind to PC3 cells much better than their nonfunctionalized counterparts.

These studies highlight the effectiveness of implementing specific binding motifs to a nanocarrier system. The use of site-specific targeting strategies would allow for more efficient delivery of cancer drugs to the tumor, and thus would reduce the amount of drug needed per dosage. More importantly, it would drastically reduce the level of toxicity to healthy cells due to nonspecific uptake. While the majority of the reviewed studies use ligands that are specific to receptors over-

expressed by cancerous cells (but still found on healthy cells) instead of using targeting ligands specific to the surface of a cancerous cell, these efforts illustrate that, in principle, the methodology is worth investigating further.

## 5. Cancer Treatment

The bulk of this review thus far has been focused on imparting functionality into carbon- and magnetic-based nanosystems for improved cancer diagnosis and treatment. Through employing any combination of highly luminescent functionality for in-vivo imaging, drug-storage capabilities, and cancer-cell specific targeting moieties, a more efficient cancer diagnostic and treatment methodology can be implemented. Moving the technology from the laboratory to the clinic is the next natural step for experimentation, and is a major research focus worldwide. The following section highlights studies wherein the previously reviewed strategies/methodologies for cancer diagnosis and treatment using nanocarrier systems are implemented and tested in vivo using animal systems.

Liu et al.<sup>[131]</sup> functionalized SWCNTs with PTX and tested its effectiveness at killing breast cancer cells in female mice. SWCNTs were functionalized with a phospholipid-branched PEG to increase biocompatibility and for higher PTX conjugation. The amine-functionalized PEG was coupled to succinic acid-modified PTX via standard coupling techniques. PTX-resistant 4T1 murine breast cancer tumors were generated by subcutaneous injection into female BALB/c mice. In-vitro cell-viability tests had shown that the SWCNT-PTX was just as effective in killing of cells as free PTX and PEG-modified PTX. The SWCNT-PTX and appropriate controls were then tested in vivo against tumors in female mice. After a 22 day testing period, the SWCNT-PTX treated tumors exhibit a ≈5-fold decrease in tumor growth compared to untreated and SWCNT-treated mice, and nearly a 4-fold decrease when compared to free PTX and PEG-modified PTX. Further

assay analysis discovered that SWCNT-PTX were more efficient at inhibiting tumor proliferation and inducing apoptosis in tumor cells. Biodistribution and organ accumulation of SWCNT-PTX was also studied. It was found that the PTX-modified SWCNTs had a circulation half-life of 1.1 h, while the circulation half-life of PEG-functionalized SWCNTs was 3.3 h. This shortened circulation time for SWCNT-PTX was attributed to the increased hydrophobic character from the PTX. SWCNT-PTX was found in higher concentrations in tumor cells than free PTX and PEG-PTX for the same dosage of PTX. Since in-vivo tumor uptake is enhanced, the amount of SWCNT-PTX could be lowered, which is beneficial for nonspecific toxicity. It is also important to note that SWCNT-PTX uptake in the blood was much higher after a 2 h period, whereas a large concentration of free PTX was found in the kidney and liver. Free SWCNTs were found to accumulate in the liver and spleen at a much higher concentration than free PTX, which was attributed to the cleaving of PTX from SWCNTs in other tissues.

Bhirde et al.<sup>[132]</sup> developed a CNT nanocarrier for targeted delivery of cancer therapeutics to head and neck squamous carcinoma cells (HNSCC) in vivo. Epidermal growth factor (EGF) was used as a targeting ligand for EGF receptors (EGFR), which are overexpressed in HNSCC. Cisplatin was used as the cancer therapeutic. Both cisplatin and EGF were conjugated onto carboxylic acid-functionalized SWCNTs using conventional coupling strategies. QDs were coupled to EGF-SWCNT for in-vitro imaging purposes. It was found that QD luminescence was only observed in HNSCC cells with EGFR rather than in those without (EGFR was

removed from the HNSCC via siRNA). Over 75% of EGFR-expressing HNSCCs internalized the nanocarriers, while less than 20% of the zero or lower-level EGFR-expressing HNSCCs had nanocarriers present. These results were verified in vivo using two-photon video imaging and confocal microscopy. In-vitro targeting experiments demonstrated that EGF-modified SWCNT-cisplatin was effective at killing cells that overexpressed EGFR. Cells not expressing EGFR had healthy cell viability. Controls of 10  $\mu\text{M}$  cisplatin, SWCNTs, EGF-SWCNTs, and SWCNT-cisplatin, had no effect on any of the cells tested. Its noteworthy that fully modified nanocarriers, with a cisplatin concentration of 1.3  $\mu\text{M}$ , were much more effective at inducing cell death than a nearly 10-fold increase of free cisplatin. In-vivo studies were performed in nude mice bearing HN12 cells that over-express EGFR. The nanocarrier and appropriate controls were injected in the tail of the mouse once the tumor had grown between 7–10 mm. Mice treated with the targeted SWCNTs exhibited a pronounced decrease in tumor growth while SWCNTs without EGF did not, illustrating the importance of implementing a targeting ligand on the nanocarrier (Figure 14a). Raman spectroscopy of tumor cryosections treated with the targeted SWCNTs had the signature G-band of SWCNTs, while the control group did not (Figure 14b). Using TEM, it was also shown that SWCNTs were present in the cross sections of tumors treated with EGF-SWCNTs (Figure 14c). Tumor cells treated with the control CNTs did not show CNTs within the cells under TEM (Figure 14d). QD-conjugated nanocarriers were not test in-vivo, but could potentially be used for targeted treatment and diagnosis.

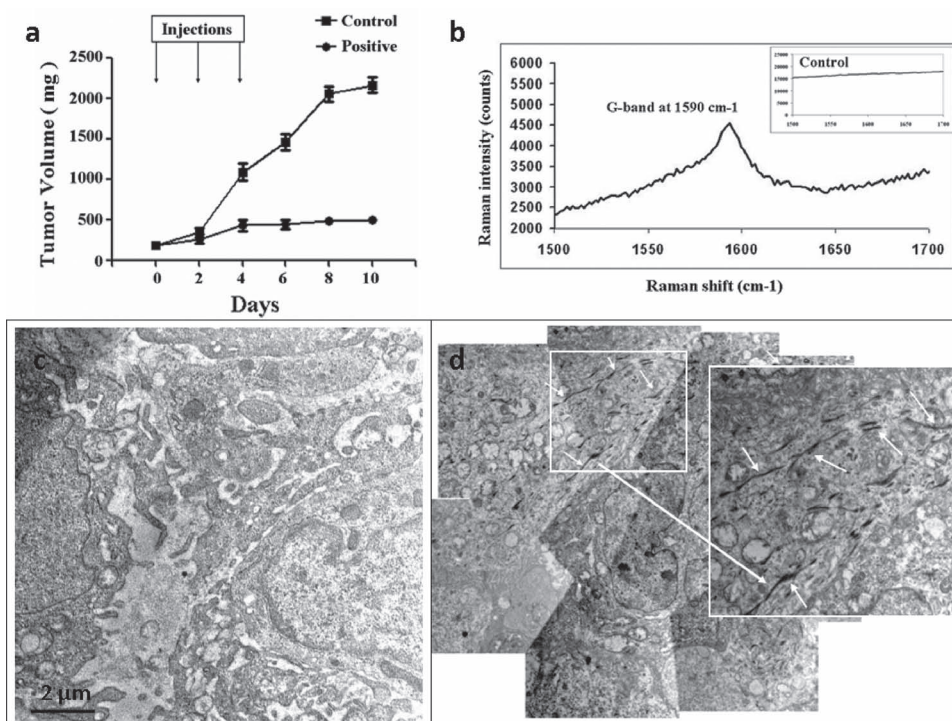


**Figure 14.** HN12 HNSCC tumor treatment with targeted nanocarriers in vivo. a) Plot showing suppressed tumor growth with targeted nanocarriers while tumors grew linearly when treated with the nontargeted nanocarriers; b) Raman spectra of tumor cryosections of tumors treated with nontargeted and targeted nanocarriers. TEM micrographs are shown in (c) and (d) respectively. Inset in (d) is a higher-magnification image showing the presence of CNTs. Reproduced with permission.<sup>[132]</sup> Copyright ACS, 2009.

An MNP system for the specific targeting and magnetic extraction of ovarian cancer cells was developed by Scarberry et al.<sup>[133]</sup> Highly magnetic cobalt spinel ferrite particles,  $\text{CoFe}_2\text{O}_4$ , were coated with polygalacturonic acid and conjugated to YSA peptide (GGGGYSAYPDSVP-MMSK) through the lysine at the C-terminus via amine-carboxylic acid coupling chemistry. YSA is an ephrin mimetic peptide that binds specifically the receptor tyrosine kinase EphA2,<sup>[134]</sup> a receptor that is overexpressed in ovarian cancer cells.<sup>[135]</sup> Magnetic nanoparticle-YSA conjugates were further tagged with a rhodamine dye at 610 nm for fluorescence observations. A continuous-flow system with EphA2-expressing cells was used to determine if the functionalized magnetic nanoparticles could extract cells from a nonstatic medium. After the inclusion of functionalized MNPs to system, cells aggregated to one side of the circulator when a magnet was present. After removal of the magnetic field, the agglomerated cellular mass redispersed back into the circulating stream. This phenomenon was not observed using magnetic nanoparticles without YSA. Similar results were obtained by incubating the nanocarrier with cells, following by washing off excess nanocarriers.

In-vivo studies were carried out using fluorescent diacetate (FDA)-tagged Hey cells and FDA tagged BG-1 cells, the former of which expressed EphA2 much more than the latter. Hey cells were injected into the peritoneum of a female mouse and dispersed through the abdomen via gentle massage, followed by rhodamine-tagged magnetic nanoparticle-YSA conjugates. After a 30 s exposure to a 2600 Gauss magnet on the abdomen of the mouse, the mouse was placed under 488 nm light. A green emission can clearly be seen from the FDA-tagged Hey cells from the abdomen of the mouse and after removal of the outer abdominal skin (Figure 15a,b). The excitation light source was then switched to 530 nm, and a red emission could be seen from the magnetic nanoparticles in the same location as the Hey cells (Figure 15c). Bright-field imaging shows a dark mass in the same area as the red emission, which is consistent for magnetic nanoparticles (Figure 15d). The same study was conducted on BG-1 cells. Green fluorescence from the BG-1 could not be seen directly from the abdomen of the mouse (Figure 15e), and was only detectable once the outer abdominal skin was removed (Figure 15f). Red fluorescence from the magnetic nanoparticles was clearly visible

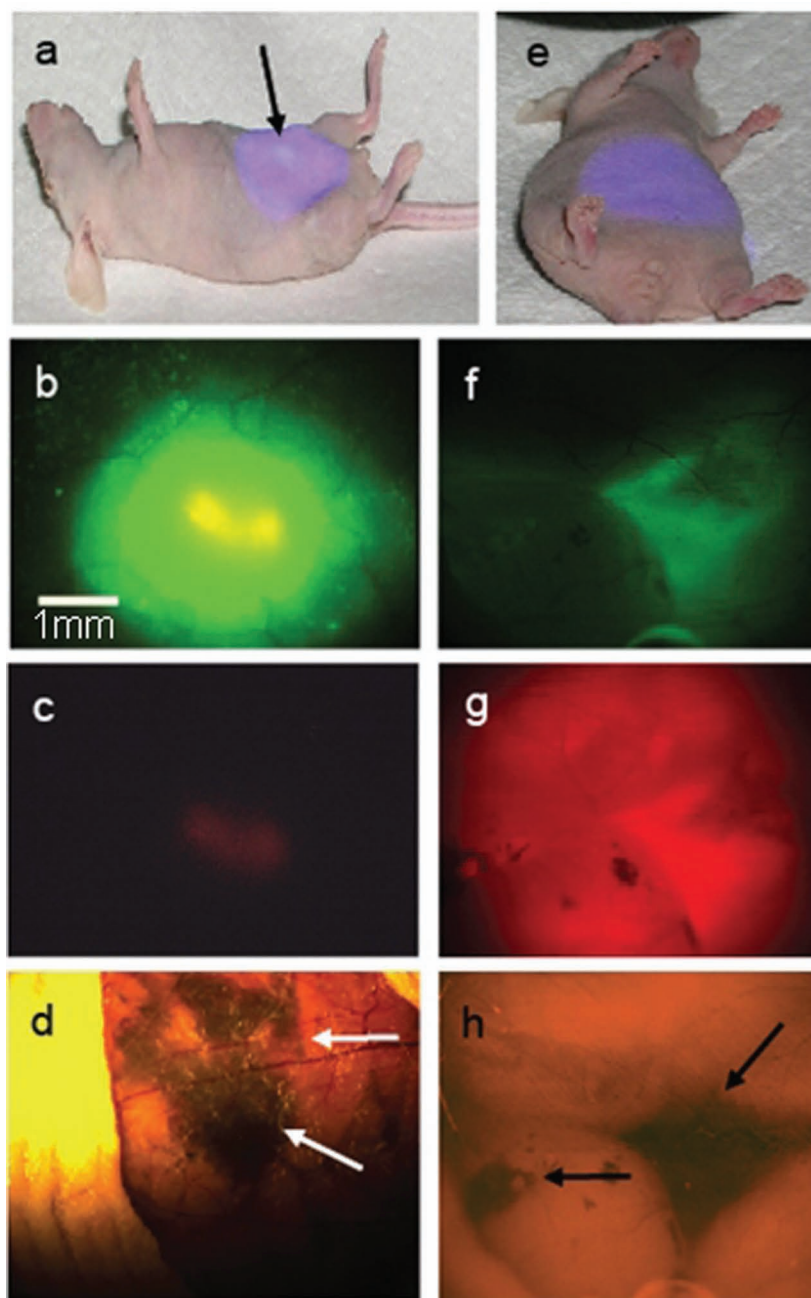


**Figure 15.** In-vivo targeting studies of Hey and BG-1 cells with MNPs. a) Green fluorescence from dye-loaded Hey cells seen through the abdominal skin of an anesthetized mouse; b) closer view of the dye-loaded Hey cells; c) red emission from the MNPs at the same site of Hey cells seen in (b); d) MNPs observed through the peritoneum at the site of the magnet; e) no visible detection of dye-loaded BG-1 through the abdominal skin of an anesthetized mouse; f) close view of the BG-1 cells after removal of abdominal skin; g) red emission from the MNPs at the site shown in (f), and; h) bright-field image of MNPs at the site on BG-1 cells. Reproduced with permission.<sup>[133]</sup> Copyright ACS, 2009.

from dark- and bright-field images (Figure 15g,h). As such, the lack of cell signal was not due to the lack of nanocarriers, but to the lack of binding between the low-EphA2-expressing BG-1 cells and the MNPs. The extraction efficiencies of the MNPs to Hey and BG-1 cells were also tested in vivo by mixing equal amounts of two cell lines and introducing them in the peritoneal cavity of mice. After incubation with the

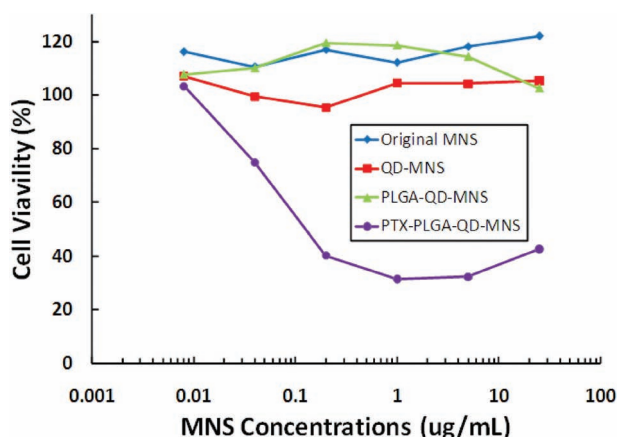


Figure 16. Dose-dependent effects of MNSs, QD-MNSs, PLGA-QD-MNS, and PTX-PLGA-QD-MNSs on human PC3mm2 prostate-cancer cell viability over a 96 h period. Reproduced with permission.<sup>[136]</sup> Copyright ACS, 2010.

MNPs, the cell extracts were filtered magnetically and found that 95–100% of the extract cells were Hey cells.

Cho et al.<sup>[136]</sup> combined fluorescent, superparamagnetic, drug-storage, and targeting functionalities into a MNS nanocarrier. Previously reported fluorescent MNSs<sup>[94]</sup> were loaded with PTX and tested for their cancer-killing ability against human metastatic PC3mm2 prostate cancer cells (Figure 16) in vitro. After a 96 h incubation period, the PTX-loaded MNSs illustrated sufficient cellular death at a concentration of 0.1  $\mu\text{g mL}^{-1}$ , while cells treated with nondrug-loaded MNS controls maintained constant cell viability. The MNSs were further functionalized with an antibody against the prostate-specific membrane antigen (antiPSMA) using conventional coupling chemistry, as depicted in Figure 17. Antibody-functionalized MNSs and nonspecific MNSs were incubated with LNCaP (PSMA-positive) and PC3mm2 (PSMA-negative) prostate-cancer cells. From Figure 18, it can be clearly seen that LNCaP cells treated with antibody-functionalized MNSs show fluorescence from the QDs coupled to the MNSs. The same cells do not exhibit luminescence when treated with nontargeted MNSs.

The PSMA-negative PC3mm2 cells exhibited no fluorescence for the antibody- and nonantibody-functionalized MNSs. In-vivo experiments were performed by injecting the targeted MNSs and control MNSs through the tail vein of tumor-bearing nude mice. Various organs of the mice were harvested and analyzed ex vivo. Untreated organs exhibited some autofluorescence in the liver, kidney, spleen, and lungs, but not as much from the tumor (Figure 19). In the antiPSMA-functionalized MNSs, the emission from the tumor region is greatly enhanced, showing that in-vivo targeting of tumor cells was successfully accomplished.

Dong et al. treated MCG-7 breast-cancer cells using sensitized, water-soluble NGO in vitro for cancer phototherapy applications.<sup>[137]</sup> NGO was functionalized with PEG and loaded with the photosensitizer zinc phthalocyanine (ZnPc) through hydrophobic and  $\pi$ - $\pi$  stacking interactions. The PEG-NGO was shown to be nontoxic to MCG-7 cells at concentrations as high as 250  $\text{mg L}^{-1}$ . PEG-NGO/ZnPc-treated cells showed, upon UV irradiation, a pronounced cytotoxicity attributed to the ZnPc photosensitizer (Figure 20). No information was given on the effect of UV light alone. Yang et al.<sup>[138]</sup> also used water-soluble NGS for the photothermal therapy of tumor-bearing mice in vivo. NGSs were rendered water-soluble with amine-functionalized PEG followed by the covalent coupling of Cy7, an IR-fluorescent dye. Figure 21 shows the in-vivo imaging of mice with various tumors injected with the

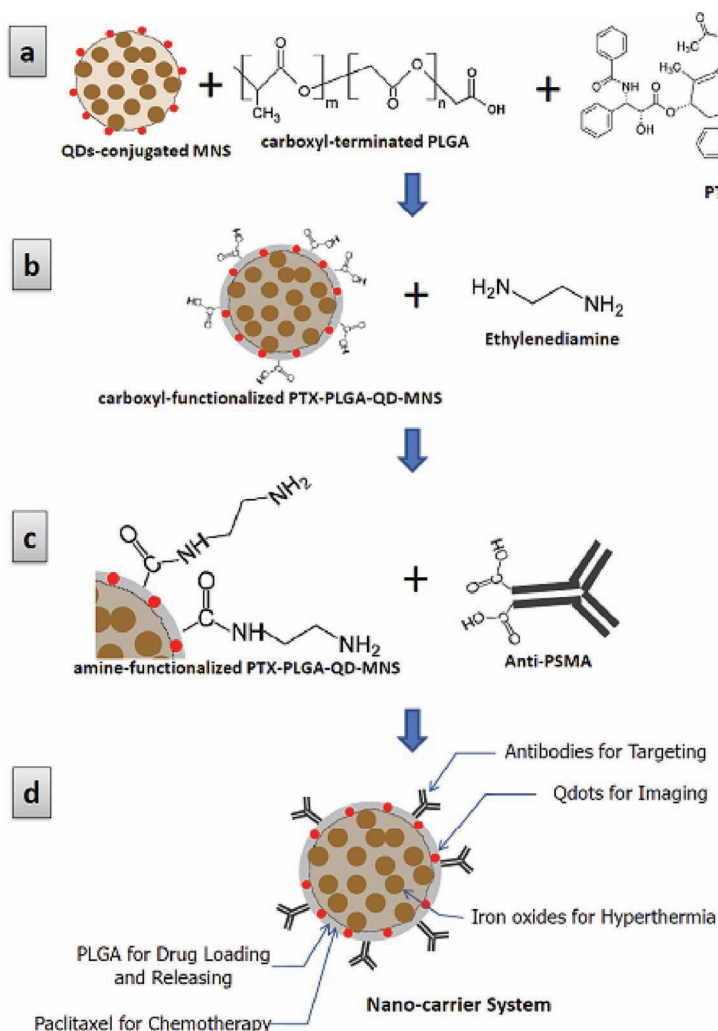
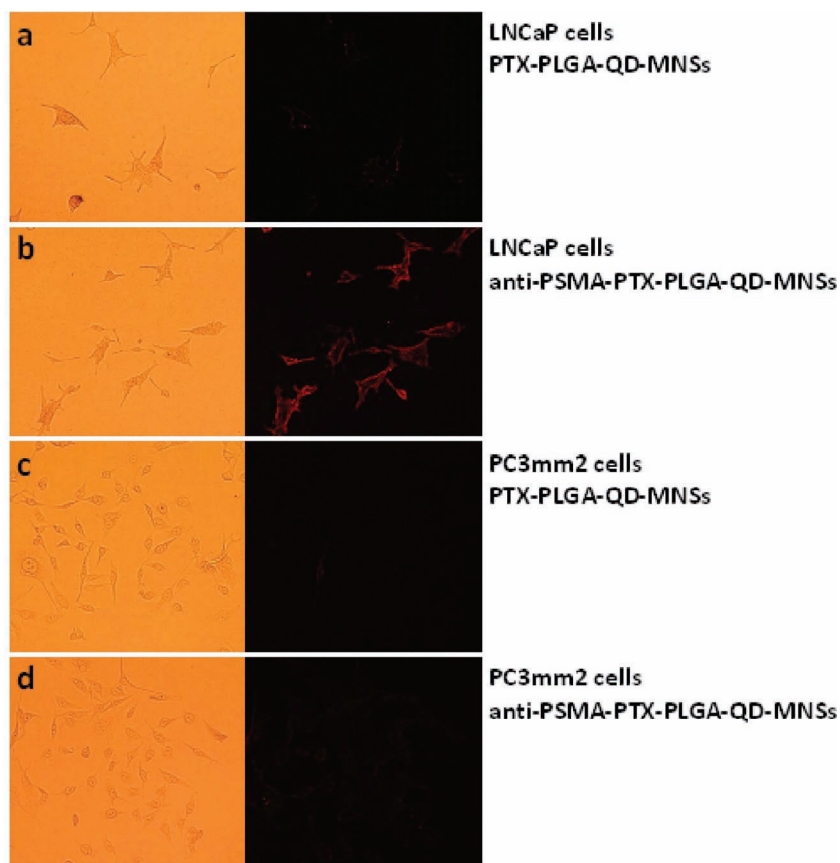
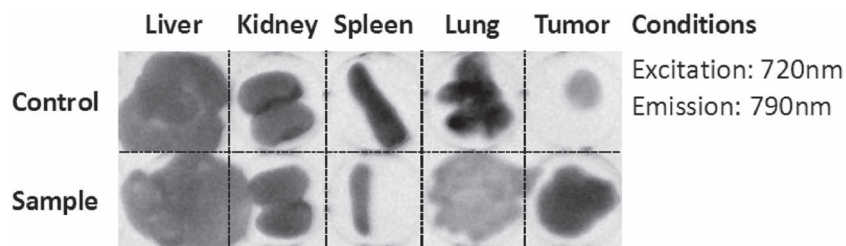


Figure 17. Schematic of the surface functionalization of antibodies onto MNSs. (a) Carboxylic acid functionality provided by the end groups of PLGA. (b) conventional EDC/NHS coupling chemistry of carboxylic acids to ethylenediamine to yield an amine functionalized MNSs, (c) conjugation of the anti-PSMA to the MNSs through EDC/NHS coupling, and (d) resulting multifunctional nanocarrier system. Reproduced with permission.<sup>[136]</sup> Copyright ACS, 2010.



**Figure 18.** In-vitro targeting studies of MNS nanocarriers against LNCaP prostate-cancer cells (PSMA-positive) and PC3mm2 (PSMA-negative). Reproduced with permission.<sup>[136]</sup> Copyright ACS, 2010.



**Figure 19.** Fluorescence images of removed organs from mice injected with targeted nanocarriers and untreated controls. Reproduced with permission.<sup>[136]</sup> Copyright ACS, 2010.

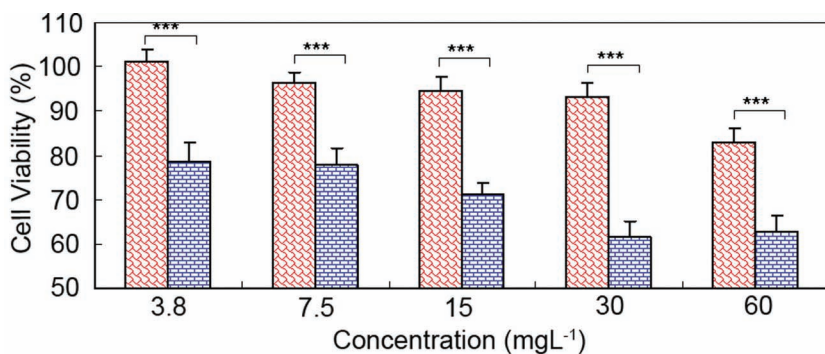


**Figure 20.** Cell viability assay at different concentrations of photosensitized NGO on MCF-7 cells under 10 min light exposure (blue bars, 60 J cm<sup>-2</sup>) and without light irradiation (red bars). Reproduced with permission.<sup>[137]</sup> Copyright Springer, 2010.

nanocarrier at various time points. A high signal from Cy7 can be seen accumulating in the tumor region for all three tumors tested after 1–6 h after injection. A biodistribution analysis determined that after a 6 h period, the only significant uptake of the NGSs was in the tumor and kidneys for 4T1 tumor-cell-bearing mice. This is particularly interesting as no target-specific ligand was functionalized onto the NGS. The photo thermal therapy studies are shown in **Figure 22** for 4T1 tumor-bearing mice. Tumor volume only ceased to increase when NGSs were present and exposed to an IR laser. All controls illustrated typical tumor growth. Of the ten mice tested in the laser + NGS group, all ten survived over a 40 day period. This again shows the potential of using graphene-based nanocarriers for cancer treatment.

## 6. Outlook

While still in its infancy, significant progress has been made in using nano-scale carbon-based materials and magnetic nanomaterials for cancer treatment and diagnosis. The use of highly luminescent materials within a nanocarrier system would allow for deep tissue optical imaging of small sized tumors. The ability to make the nanocarriers biocompatible while simultaneously carrying anti-cancer therapeutics is also beneficial as it increases drug dose-per-unit-volume in aqueous media, which can in turn increase the efficiency by which the drug is administered. The use of specific targeting ligands further increases this efficiency while minimizing the toxic effects of cancer treatment by localizing the nanocarrier to cancerous cells, thus reducing the uptake of cancer drugs in healthy cells. Magnetically active nanocarriers have the added ability to be localized via an external magnetic field while simultaneously being implemented as a therapeutic agent through magnetic hyperthermia. The use of phototherapy techniques is also of interest due to the ease at which a tumor can be subjected to an external light source for localized treatment.

Using intelligently engineered nanocarrier systems, in-vivo imaging, drug delivery, drug release, biocompatibility, specific targeting, magnetic hyperthermia, and/or phototherapy characteristics can be

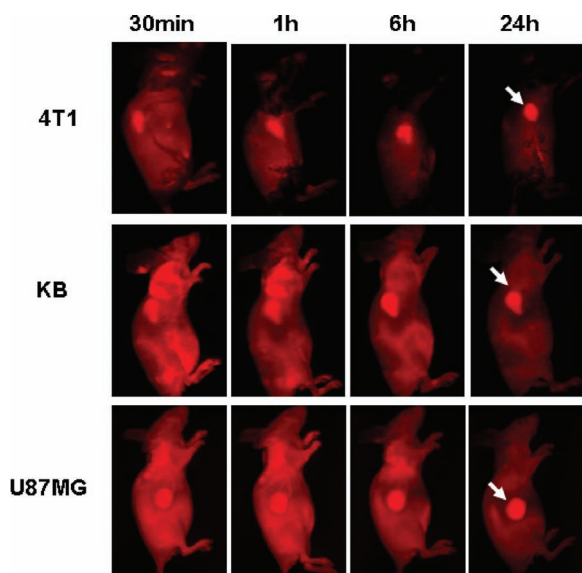


Figure 21. In-vivo images of 4T1 tumor-bearing Balb/c mice, KB, and U87MG tumor-bearing nude mice at different time points after injection of an NGS-based nanocarrier system. Reproduced with permission.<sup>[138]</sup> Copyright ACS, 2010.

advantageously utilized to better locate and treat cancer cells. While the bulk of this review focused on CNTs and MNSs, the use of graphene-based nanocarriers should be explored further, especially considering the encouraging results from Liu et al.<sup>[112]</sup> and Yang et al.<sup>[138]</sup> Further advancement of the field will require an increased interdisciplinary collaboration from research groups consisting of materials scientists, physicians, chemists, microbiologists, and physicists. Yet for any type of nanocarrier system to be successful in human trials, and to become ubiquitous in the clinical domain, key areas need to be addressed; improved developments of real-time in-vivo imaging and, perhaps more importantly, employing targeting ligands that show specificity to particular cancer cell lines. Overcoming such challenges would be key milestones to achieve in order to make cancer treatment and diagnosis more efficient and less toxic overall.

A major issue with in-vivo optical imaging is the natural autofluorescence from biological tissues and fluids. Particular to mice models, the autofluorescence is largely attributed to the chlorophyll found in the diets of many animal models. This issue could potentially be amplified in human imaging given the comparative complexity and variation of human diets. Figure 23 is a good example of how

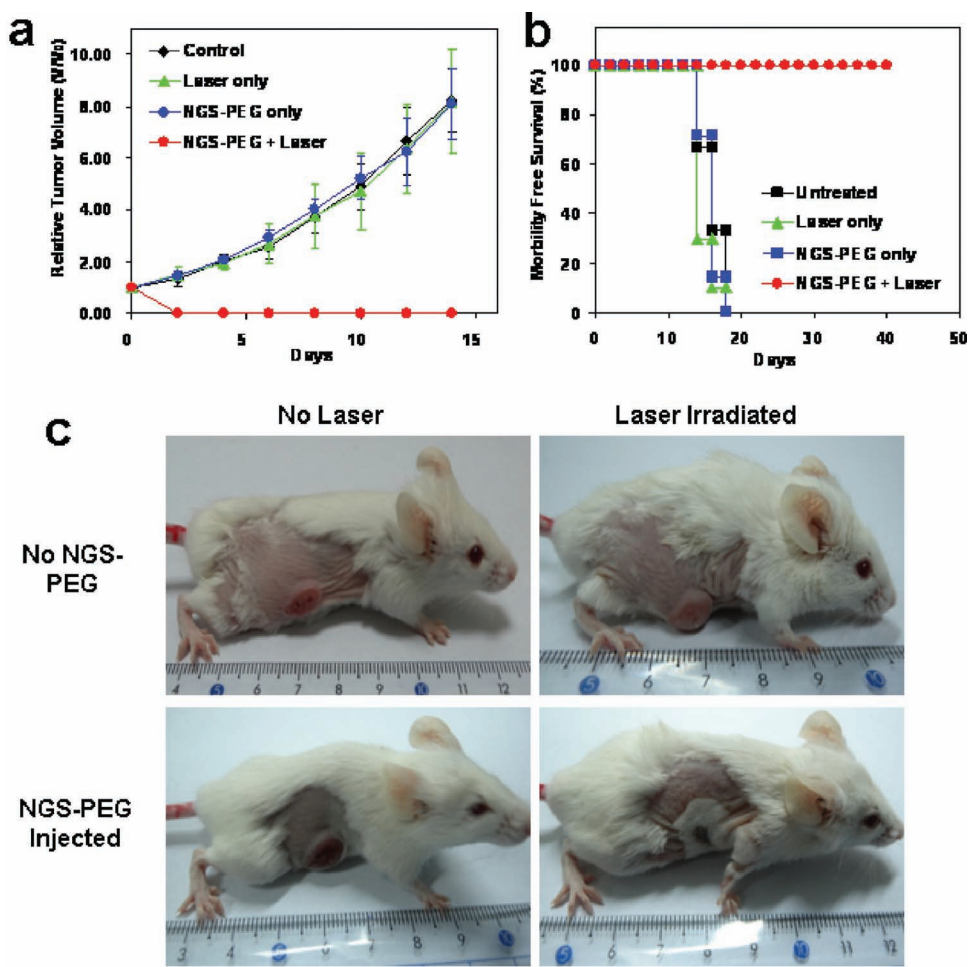
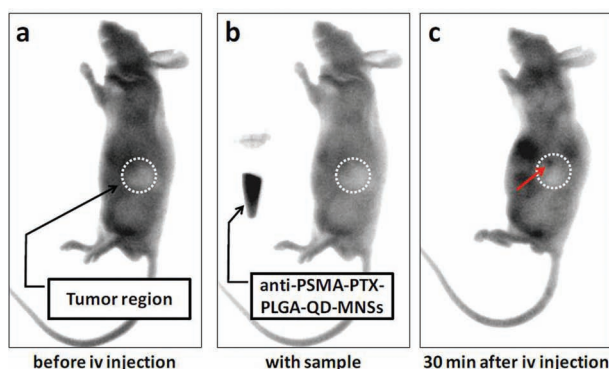


Figure 22. In-vivo photothermal therapy study of NGS based nanocarriers. a) Tumor growth curves for nanocarrier treatment and appropriate controls; b) survival curves of mice bearing 4T1 tumors during the treatments seen in (a), and; c) representative photos of tumors on mice after various treatments. Reproduced with permission.<sup>[138]</sup> Copyright ACS, 2010.



**Figure 23.** Grayscale in-vivo fluorescence images of a) a mouse before IV injection of fluorescent targeted nanocarriers, b) comparative fluorescence of nanocarriers, and c) 30 min post injection.

problematic autofluorescence can be in interpreting in-vivo images. Figure 23a shows the grayscale in-vivo fluorescence images of the mouse prior to intravenous injection of fluorescent tumor-targeting MNSs discussed in reference [136] showing an inherent autofluorescence. The cancerous region of the mouse is highlighted. For comparison purposes, a grayscale image of the mouse next to a vial of the nanocarriers is shown in Figure 23b. Figure 23c shows the mouse 30 min after injection of the nanocarrier system. The red arrow shows an increase fluorescence in the tumor region, but similar in signal to areas throughout the mouse. Only after ex-vivo imaging of the tumor and various organs could successfully specific targeting be confirmed (Figure 19). Such issues with diet and autofluorescence have been previously studied,<sup>[139–142]</sup> but it is still not fully understood how changes in diet affect autofluorescence in rodent models and if such approaches will ever fully remove autofluorescence. Further investigation is needed to overcome this issue, as well as studying brighter emitting nanocarriers and/or nanocarriers that emit at even longer wavelengths.

The targeting strategies more commonly used in the field of nano-biomedicine (including those mentioned in this review), while initially show promise, may not be selective enough for cancer treatment. Simply using ligands that bind to cell receptors overexpressed in cancer cells but still present in health cells may still lead to nonspecific uptake and thus may not circumvent the toxicity issues seen in classical cancer treatment. One potential route that needs increased exploration is the coupling of peptides and DNA/RNA aptamers discovered through phage display<sup>[143–147]</sup> or SELEX<sup>[148–151]</sup> techniques with a nanocarrier. These panning procedures yield specific peptide or aptamers sequences specific only to the analyte tested, which in the referenced examples are cancerous cells. Such peptides and aptamers could be readily tethered to a nanocarrier system via covalent coupling strategies. Alternatively, a two-domain peptide or aptamer could be used in which one domain would bind to the nanocarrier, while the other domain is used as a targeting ligand. This would forgo the need to perform additional chemistry while removing defects in the nanocarrier caused by covalent coupling chemistry. Sequences have already been

discovered for the selective binding of CNTs,<sup>[152,153]</sup> Fe<sub>3</sub>O<sub>4</sub>,<sup>[154]</sup> and graphene.<sup>[155]</sup> Two-domain peptides are already receiving much attention in the materials science community for usage largely in sensor applications.<sup>[156,157]</sup>

Multifunctional nanocarriers designed with advantageous characteristics for early cancer diagnosis and localized, targeted treatment could potentially result in a paradigm shift in wide-scale cancer therapeutics. The next phase of nano-biomedicine may be to include functionalities for temporally responsive triggers. That is, a more ‘evolved’ nanocarrier could provide the functionalities previously discussed in this review but also response to changes in the cellular environment and react in a predetermined manner. For example, if a nanocarrier provoked an immune response in the body it could trigger an action from the nanocarrier to evade such a response. Another example would be to trigger a nanocarrier to impede or stop the release of cancer drugs once the presence of certain biomarkers for cancer cell apoptosis are present in the environment. Such next-generation nanocarriers, carbon- and/or magnetic-based, would further advance an already promising field of nano-biomedicine.

## Acknowledgements

The authors would collectively like to thank Dr. Giovanni Pauletti and Chris Huth (University of Cincinnati) for their critical review and editing of this manuscript. The authors are grateful to Dr. Haiqing Dong for developing the schematic drawing of Figure 1. We would also like to thank Drs. San-Yuan Chen (National Chiao Tung University), Hongjie Dai (Stanford University), Qinghua Lu (Shanghai Jiao Tong University), James F. Rusling (University of Connecticut), Z. John Zhang (Georgia Institute of Technology), and Zhuang Liu (Soochow University) for kindly provides figures for this review. N.M. Bedford would like to acknowledge the financial support from the Dayton Area Graduate Studies Institute.

- [1] H. Lee, T.-J. Yoon, J.-L. Figueiredo, F. K. Swirski, R. Weissleder, *Proc. Natl. Acad. Sci. USA* **2009**, *106*, 12459.
- [2] A. Villers, L. Lemaitre, J. Haffner, P. Puech, *Curr. Opin. Urol.* **2009**, *19*, 274.
- [3] K. H. Barck, B. Willis, J. Ross, D. M. French, E. H. Filvaroff, A. D. Carano, *Magn. Reson. Med.* **2009**, *62*, 1423.
- [4] H. Degani, V. Gusic, D. Weinstein, S. Fields, S. Strano, *Nat. Med.* **1997**, *3*, 780.
- [5] S. H. Heywang-KoBrunner, R. W. Katzberg, *Invest. Radiol.* **1994**, *29*, 94.
- [6] W. A. Kaiser, E. Zeitler, *Radiology* **1989**, *170*, 681.
- [7] D. Shi, *Adv. Funct. Mater.* **2009**, *19*, 3356.
- [8] S. M. Chung, *J. Neuro-Ophthalmol.* **2002**, *22*, 35.
- [9] F. G. Shellock, *J. Magn. Reson. Imaging* **2002**, *16*, 721.
- [10] P. Nordbeck, I. Weiss, P. Ehse, O. Ritter, M. Warmuth, F. Fidler, V. Herold, P. M. Jakob, M. E. Ladd, H. H. Quick, W. R. Bauer *Magn. Reson. Med.* **2009**, *61*, 570.
- [11] C. M. Carpenter, B. W. Pogue, S. Jiang, H. Dehghani, X. Wang, K. D. Paulsen, W. A. Wells, J. Forero, C. Kogel, J. B. Weaver, S. P. Poplack, *Opt. Lett.* **2007**, *32*, 933.

- [12] A. M. Winkler, P. F. S. Rice, R. A. Drezek, J. K. Barton, *J. Biomed. Opt.* **2010**, *15*, 041512.
- [13] L. P. Hariri, G. T. Bonnema, K. Schmidt, A. M. Winkler, V. Korde, K. D. Hatch, J. R. Davis, M. A. Brewer, J. K. Barton, *Gynecol. Oncol.* **2009**, *114*, 188.
- [14] L. P. Hariri, Z. Qiu, A. R. Tumlinson, D. G. Besselsen, E. W. Gerner, N. A. Ignatenko, B. Považay, B. Hermann, H. Sattmann, J. McNally, A. Unterhuber, W. Drexler, J. K. Barton, *Cancer Bio. Ther.* **2007**, *6*, 1753.
- [15] A. Corlu, R. Choe, T. Durduran, M. A. Rosen, M. Schweiger, S. R. Arridge, M. D. Schnall, A. G. Yodh, *Opt. Express* **2007**, *15*, 6696.
- [16] R. Choe, A. Corlu, K. Lee, T. Durduran, S. D. Konecky, M. Grosicka-Koptyra, S. R. Arridge, B. J. Czerniecki, D. L. Fraker, A. DeMichele, B. Chance, M. A. Rosen, A. G. Yodh, *Med. Phys.* **2005**, *32*, 1128.
- [17] J. S. de Bono, A. Ashworth, *Nature* **2010**, *467*, 543.
- [18] A. Villar-Gerea, M. Esteller, *Curr. Drug Metab.* **2003**, *4*, 11.
- [19] G. Bergers, D. Hanahan, *Nat. Rev. Cancer.* **2008**, *8*, 592.
- [20] B. Han, J.-T. Zhang, *Curr. Med. Chem. Anticancer Agents* **2004**, *4*, 31.
- [21] Y. Matsumura, H. Maeda, *Cancer Res.* **1986**, *46*, 6387.
- [22] A. K. Iyer, G. Khaled, J. Fang, H. Maeda, *Drug Discovery Today* **2006**, *11*, 813.
- [23] H. Maeda, J. Wu, T. Sawa, Y. Matsumura, K. Hori, *J. Control. Release* **2000**, *65*, 271.
- [24] M. Das, C. Mohanty, S. K. Sahoo, *Expert Opin. Drug Deliv.* **2009**, *6*, 285.
- [25] R. L. Schilshky, *Nat. Rev. Drug Discov.* **2010**, *9*, 363.
- [26] D. Schrama, R. A. Reisfeld, J. C. Becker, *Nat. Rev. Drug Discov.* **2006**, *5*, 147.
- [27] W. Tai, R. Mahato, K. Cheng, *J. Control. Release* **2010**, *145*, 264.
- [28] H.-Y. Wen, H.-Q. Dong, W.-j. Xie, Y.-Y. Li, K. Wang, G. M. Pauletti, D. Shi, *Chem. Comm.* **2011**, *47*, 3550.
- [29] A. S. Lübbe, C. Bergemann, W. Huhnt, T. Fricke, H. Riess, J. W. Brock, D. Huhn, *Cancer Res.* **1996**, *56*, 4694.
- [30] A. S. Lübbe, C. Alexiou, C. Bergemann, *J. Sur. Res.* **2001**, *95*, 200.
- [31] R. Tietze, R. Jurgons, S. Lyer, E. Schreiber, F. Wiekhorst, D. Eberbeck, H. Richter, U. Steinhoff, L. Trahms, C. Alexiou, *J. Magn. Magn. Mater.* **2009**, *321*, 1465.
- [32] R. Hergt, S. Dutz, R. Muller, M. Zeisberger, *J. Phys.: Condens. Matter* **2006**, *18*, S2919.
- [33] F. Sonvico, S. Mornet, S. Vasseur, C. Dubernet, D. Jaillard, J. Degrouard, J. Hoebeke, E. Duguet, P. Colombo, P. Couvreur, *Bioconjugate Chem.* **2005**, *16*, 1181.
- [34] C. C. Berry, A. S. G. Curtis, *J. Phys. D: Appl. Phys.* **2003**, *36*, R198.
- [35] S. Mornet, S. Vasseur, F. Grasset, E. Duguet, *J. Mater. Chem.* **2004**, *14*, 2161.
- [36] D. C. F. Chan, D. B. Kirpotin, P. A. Bunn Jr, *J. Magn. Magn. Mater.* **1993**, *122*, 374.
- [37] K. Maier-Hauff, R. Rothe, R. Scholz, U. Gneveckow, P. Wust, B. Thiesen, A. Feussner, A. von Deimling, N. Waldoefner, R. Felix, A. Jordan, *J. Neurooncol.* **2007**, *81*, 53.
- [38] M. Johannsen, U. Gneveckow, B. Thiesen, K. Taymoorian, C. H. Cho, N. Waldöfner, R. Scholz, A. Jordan, S. A. Loening, P. Wust, *Eur. Urol.* **2007**, *52*, 1653.
- [39] Y. Ikehara, T. Niwa, L. Biao, S. K. Ikehara, N. Ohashi, T. Kobayashi, Y. Shimizu, N. Kojima, H. Nakanishi, *Cancer Res.* **2006**, *66*, 8740.
- [40] S.-H. Hu, D.-M. Liu, W.-L. Tung, C.-F. Liao, S.-Y. Chen, *Adv. Funct. Mater.* **2008**, *18*, 2946.
- [41] A. M. Derfus, G. von Maltzahn, T. J. Harris, T. Duza, K. S. Vecchio, E. Ruoslahti, S. N. Bhatia, *Adv. Mater.* **2007**, *19*, 3932.
- [42] C. R. Thomas, D. P. Ferris, J.-H. Lee, E. Choi, M. H. Cho, E. S. Kim, J. F. Stoddart, J.-S. Shin, J. Cheon, J. I. Zink, *J. Amer. Chem. Soc.* **2010**, *132*, 10623.
- [43] K. Hayashi, K. Ono, H. Suzuki, M. Sawada, M. Moriya, W. Sakamoto, T. Yogo, *ACS Appl. Mater. Interfaces* **2010**, *2*, 1903.
- [44] P. V. Finotelli, D. Da Silva, M. Sola-Penna, A. M. Rossi, M. Farina, L. R. Andrade, A. Y. Takeuchi, M. H. Rocha-Leão, *Colloids Surf. B: Biointerfaces.* **2010**, *81*, 206.
- [45] A. Peigney, C. Laurent, E. Flahaut, A. Rousset, *Ceram. Int.* **2000**, *26*, 677.
- [46] H. Cho, D. Shi, Y. Guo, J. Lian, Z. Ren, B. Poudel, Y. Song, J. L. Abot, D. Singh, J. Routbort, L. Wang, R. C. Ewing, *Adv. Mater.* **2008**, *104*, 074302.
- [47] I. Carmeli, M. Mangold, L. Frolov, B. Zebli, C. Carmeli, S. Richter, A. W. Holleitner, *Adv. Mater.* **2007**, *19*, 3901.
- [48] M. Ding, Y. Tang, P. Gou, M. J. Reber, A. Star, *Adv. Mater.* **2011**, *23*, 536.
- [49] Y. Zhao, G. Xing, Z. Chai, *Nat. Nanotechnol.* **2008**, *3*, 191.
- [50] K. Kostarelos, *Nat. Biotechnol.* **2008**, *7*, 774.
- [51] C. A. Poland, R. Duffin, I. Kinloch, A. Maynard, W. A. H. Wallace, A. Seaton, V. Stone, S. Brown, W. MacNee, K. Donaldson, *Nat. Nanotechnol.* **2008**, *3*, 423.
- [52] J. Muller, I. Docordier, P. H. Hoet, N. Lombaert, L. Thomassen, F. Huaux, D. Lison, M. Kirsch-Volders, *Carcinogenesis* **2008**, *29*, 427.
- [53] M. Bottini, S. Bruckner, K. Nika, N. Bottini, S. Bellucci, A. Magrini, A. Bergamaschi, T. Mustelin, *Toxicol. Lett.* **2006**, *160*, 121.
- [54] J. Kayat, V. Gajbhiye, R. K. Tekade, N. K. Jain, *Nanomed. Nanotechnol. Biol. Med.* **2011**, *7*, 40.
- [55] H. Dumortier, S. Lacotte, G. Pastorin, R. Marega, W. Wu, D. Bonifazi, J.-P. Briand, M. Prato, S. Muller, A. Bianco, *Nano Lett.* **2006**, *6*, 1522.
- [56] M. L. Schipper, N. Nakayama-Ratchford, C. R. Davis, N. W. Shi Kam, P. Chu, Z. Liu, X. Sun, H. Dai, S. S. Gambhir, *Nat. Nanotechnol.* **2008**, *3*, 216.
- [57] X. Deng, F. Wu, Z. Liu, M. Luo, L. Li, Q. Ni, Z. Jiao, M. Wu, Y. Liu, *Carbon* **2009**, *47*, 1421.
- [58] H. Zhou, Q. Mu, N. Gao, A. Liu, Y. Xing, S. Gao, Q. Zhang, G. Qu, Y. Chen, G. Liu, B. Zhang, B. Yan, *Nano Lett.* **2008**, *8*, 859.
- [59] Y. Bai, Y. Zhang, J. Zhang, Q. Mu, W. Zhang, E. R. Butch, S. E. Snyder, B. Yan, *Nat. Nanotechnol.* **2010**, *5*, 683.
- [60] T. K. Jain, M. K. Reddy, M. A. Morales, D. L. Leslie-Pelecky, V. Labhasetwar, *Mol. Pharm.* **2008**, *5*, 316.
- [61] S. A. Meenach, A. A. Anderson, M. Suthar, K. W. Anderson, Z. Hilt, *J. Biomed. Mater. Res. Part A.* **2009**, *91*, 903.
- [62] M. Mahmoudi, A. Simchi, A. S. Milani, P. Stroeve, *J. Coll. Interface Sci.* **2009**, *336*, 510.
- [63] R. Qiao, C. Yang, M. Gao, *J. Mater. Chem.* **2009**, *19*, 6274.
- [64] K. Yang, J. Wen, S. Zhang, Y. Zhang, S.-T. Lee, Z. Liu, *ACS Nano* **2011**, *5*, 516.
- [65] Y. Chang, S.-T. Yang, J.-H. Liu, E. Dong, Y. Wang, A. Cao, Y. Liu, H. Wang, *Toxicol. Lett.* **2011**, *200*, 201.
- [66] Y. Guo, D. Shi, J. Lian, Z. Dong, W. Wang, H. Cho, G. Liu, L. Wang, R. C. Ewing, *Nanotechnol.* **2008**, *19*, 175102.
- [67] W. Wang, D. Shi, J. Lian, Y. Guo, G. Liu, L. Wang, R. C. Ewing, *Appl. Phys. Lett.* **2006**, *89*, 183106.
- [68] H. Meng, M. Llong, T. Xia, Z. Li, Z. Ji, J. I. Zink, A. E. Nel, *ACS Nano* **2010**, *4*, 4539.
- [69] M. Llong, J. Lu, M. Kovochich, T. Xia, S. G. Ruehm, A. E. Nel, F. Tamanol, J. I. Zink, *ACS Nano* **2008**, *2*, 889.
- [70] C. Oerlemans, W. Bult, M. Bos, G. Storm, J. F. W. Nigsen, W. E. Hennik, *Pharm. Res.* **2010**, *27*, 2569.
- [71] I.-S. Kim, Y.-I. Jeong, C.-S. Cho, S.-H. Kim, *Inter. J. Pharm.* **2000**, *205*, 165.
- [72] Y. Dong, S.-S. Feng, *Biomaterials* **2005**, *26*, 6068.
- [73] S. K. Sahoo, W. Ma, V. Labhasetwar, *Int. J. Cancer* **2004**, *112*, 335.
- [74] J.-H. Park, G. von Maltzahn, E. Ruoslahti, S. N. Bhatia, M. J. Sailor, *Angew. Chem. Int. Ed.* **2008**, *47*, 7284.
- [75] L. O. Cinteza, T. Y. Ohulchanskyy, Y. Sahoo, E. J. Bergey, R. K. Pandey, P. N. Prasad, *Mol. Pharm.* **2006**, *3*, 415.

- [76] A. K. Patri, I. J. Majoros, J. R. Baker, *Curr. Opin. Chem. Biol.* **2002**, *6*, 466.
- [77] D. Luo, K. Haverstick, N. Belcheva, E. Han, W. M. Saltzman, *Macromolecules* **2002**, *35*, 3456.
- [78] W. C. W. Chan, S. Nie, *Science* **1998**, *281*, 2016.
- [79] S. Kim, Y. T. Lim, E. G. Soltesz, A. M. De Grand, J. Lee, A. Nakayama, J. A. Parker, T. Mihaljevic, R. G. Laurence, D. M. Dor, L. H. Cohn, M. G. Bawendi, J. V. Frangioni, *Nat. Biotechnol.* **2004**, *22*, 93.
- [80] W. Cai, D.-W. Shin, K. Chen, O. Gheysens, Q. Cao, S. X. Wang, S. S. Gambhir, X. Chen, *Nano Lett.* **2006**, *6*, 669.
- [81] R. Huschka, O. Neumann, A. Barhoumi, N. J. Halas, *Nano Lett.* **2010**, *10*, 4117.
- [82] R. Bardhan, W. Chen, M. Bartels, C. Perez-Torres, M. F. Botero, R. W. McAninch, A. Contreras, R. Schiff, R. G. Pautler, N. J. Halas, A. Joshi, *Nano Lett.* **2010**, *10*, 4920.
- [83] P. Horcajada, T. Chalati, C. Serre, B. Gillet, C. Sebrie, T. Baati, J. F. Eubank, D. Heurtaux, P. Clayette, C. Kreuz, J.-S. Chang, Y. K. Hwang, V. Marsaud, P.-N. Bories, L. Cynober, S. Gil, G. Férey, P. Couvreur, R. Gref, *Nat. Mater.* **2010**, *9*, 172.
- [84] L. J. McCartney, J. C. Pickup, O. J. Rolinski, D. J. S. Birch, *Anal. Biochem.* **2001**, *292*, 216.
- [85] F. Wang, G. Dukovic, L. E. Burs, T. F. Heinz, *Science* **2005**, *308*, 838.
- [86] X. Gao, Y. Cui, R. M. Levenson, L. W. K. Chung, S. Nie, *Nat. Biotechnol.* **2004**, *22*, 969.
- [87] B. Dubertret, P. Skourides, D. J. Norris, V. Noireaux, A. H. Brivanlou, A. Libchaber, *Science* **2002**, *298*, 1759.
- [88] X. Wu, H. Liu, J. Liu, K. N. Haley, J. A. Treadway, J. P. Larson, N. Ge, F. Peale, M. P. Bruchez, *Nat. Biotechnol.* **2003**, *21*, 41.
- [89] L. Brus, *Appl. Phys. A* **1991**, *53*, 465.
- [90] A. P. Alivisatos, *J. Phys. Chem.* **1996**, *100*, 13226.
- [91] D. Shi, Y. Guo, Z. Dong, J. Lian, W. Wang, G. Liu, L. Wang, R. C. Ewing, *Adv. Mater.* **2007**, *19*, 4033.
- [92] D. Shi, J. Lian, P. He, L. M. Wang, W. J. van Ooij, M. Schulz, Y. Liu, D. B. Mast, *Appl. Phys. Lett.* **2002**, *81*, 5216.
- [93] D. Shi, P. He, J. Lian, L. Wang, W. J. van Ooij, *J. Mater. Res.* **2002**, *17*, 2555.
- [94] D. Shi, H. S. Cho, Y. Chen, H. Xu, H. Gu, J. Lian, W. Wang, G. Liu, C. Huth, L. Wang, R. C. Ewing, S. Budko, G. M. Pauletti, Z. Dong, *Adv. Mater.* **2009**, *21*, 2170.
- [95] Q. L. Fan, K. G. Neoh, E. T. Kang, B. Shuter, S. C. Wang, *Biomaterials* **2007**, *28*, 5426.
- [96] H. Iida, K. Takayanagi, T. Nakanishi, T. Osaka, *J. Colloid Interface Sci.* **2007**, *314*, 274.
- [97] T. Hyeon, S. S. Lee, J. Park, Y. Chung, H. B. Na, *J. Am. Chem. Soc.* **2001**, *123*, 12798.
- [98] H. Xu, L. L. Cai, N. H. Tong, H. Gu, *J. Am. Chem. Soc.* **2006**, *128*, 15582.
- [99] J. Cheng, B. A. Teplý, I. Sherifi, J. Sung, G. Luther, F. X. Gu, E. Levy-Nissenbaum, A. F. Radovic-Moreno, R. Langer, O. C. Farokhzad, *Biomaterials* **2007**, *28*, 869.
- [100] D. Shi, H. S. Cho, C. Huth, F. Wang, Z. Dong, G. M. Pauletti, J. Lian, W. Wang, G. Liu, S. L. Bud'ko, L. Wang, R. C. Ewing, *Appl. Phys. Lett.* **2009**, *95*, 223702.
- [101] W. Wang, G. K. Liu, H. S. Cho, Y. Guo, D. Shi, J. Lian, R. C. Ewing, *Chem. Phys. Lett.* **2009**, *469*, 149.
- [102] P. Howes, M. Green, A. Bowers, D. Parker, G. Varma, M. Kallumadil, M. Hughes, A. Warley, A. Brain, R. Botnar, *J. Am. Chem. Soc.* **2010**, *132*, 9833.
- [103] T. A. Larson, J. Bankson, J. Aaron, K. Sokolov, *Nanotechnol.* **2007**, *18*, 325101.
- [104] Y. T. Lim, M. Y. Cho, J. K. Kim, S. Hwangbo, B. H. Chung, *Chem-BioChem* **2007**, *8*, 2204.
- [105] Y. Guo, D. Shi, H. Cho, Z. Dong, A. Kulkarni, G. M. Pauletti, W. Wang, J. Lian, W. Liu, L. Ren, Q. Zhang, G. Liu, C. Huth, L. Wang, R. C. Ewing, *Adv. Funct. Mater.* **2008**, *18*, 2489.
- [106] C. M. Spencer, D. Faulds, *Drugs* **1994**, *48*, 794.
- [107] M. Ishitobi, E. Shin, N. Kikkawa, *Int. J. Clin. Oncol.* **2001**, *6*, 55.
- [108] S.-H. Hu, D.-M. Liu, W.-L. Tung, C.-F. Liao, S.-Y. Chen, *Adv. Funct. Mater.* **2008**, *18*, 2946.
- [109] S.-H. Hu, S.-Y. Chen, D.-M. Liu, C.-S. Hsiao, *Adv. Mater.* **2008**, *20*, 2690.
- [110] S.-H. Hu, K.-T. Kuo, W.-L. Tung, D.-M. Liu, S.-Y. Chen, *Adv. Funct. Mater.* **2009**, *19*, 3396.
- [111] W. Wang, M. Zou, K. Chen, *Chem. Commun.* **2010**, *46*, 5100.
- [112] Z. Liu, J. T. Robinson, X. Sun, H. Dai, *J. Am. Chem. Soc.* **2008**, *130*, 10876.
- [113] A. Tanizawa, A. Fujimori, Y. Fujimori, Y. Pommier, *J. Natl. Cancer Inst.* **1994**, *86*, 836.
- [114] J. G. Slatter, L. J. Schaaf, J. P. Sams, K. L. Feenstra, M. G. Johnson, P. A. Bombardt, K. S. Cathcart, M. T. Verburg, L. K. Pearson, L. D. Compton, L. L. Miller, D. S. Baker, C. V. Pesheck, R. S. Lord, *Drug Metab. Dispos.* **2000**, *28*, 423.
- [115] N. W. S. Kam, M. O'Connell, J. A. Wisdom, H. Dai, *Proc. Natl. Acad. Sci. USA* **2005**, *102*, 11600.
- [116] Y. Lu, E. Segal, C. P. Leamon, P. S. Low, *Adv. Drug Deliv. Rev.* **2004**, *56*, 1161.
- [117] N. Shao, S. Lu, E. Wickstrom, B. Panchapakesan, *Nanotechnol.* **2007**, *18*, 315101.
- [118] K. Welscher, Z. Liu, D. Daranciang, H. Dai, *Nano Lett.* **2008**, *8*, 586.
- [119] A. Rhodes, *Cancer Biomarkers* **2005**, *1*, 229.
- [120] W. P. Carney, R. Neumann, A. Lipton, K. Leitzel, S. Ali, C. P. Price, *Clin. Breast Cancer* **2004**, *5*, 105.
- [121] M. Summerhayes, *J. Oncol. Pharm. Practice* **2001**, *7*, 9.
- [122] X. Zhang, L. Meng, Q. Lu, Z. Fei, P. J. Dyson, *Biomaterials* **2009**, *30*, 6041.
- [123] R. Weissleder, A. Moore, U. Mahmood, R. Bhorade, H. Benveniste, E. A. Chiocca, J. P. Babilion, *Nat. Med.* **2000**, *6*, 351.
- [124] M. Zhao, D. A. Beaugard, L. Loizou, B. Davletov, K. M. Brindle, *Nat. Med.* **2001**, *7*, 1241.
- [125] H. W. Kang, L. Josephson, A. Petrovsky, R. Weissleder, A. Bogdanov Jr., *Bioconjugate Chem.* **2002**, *13*, 122.
- [126] Y.-w. Jun, Y.-M. Huh, J.-s. Choi, J.-H. Lee, H.-T. Song, S. Kim, S. Yoon, K.-S. Kim, J.-S. Shin, J.-S. Suh, J. Cheon, *J. Am. Chem. Soc.* **2005**, *127*, 5732.
- [127] S. C. Wuang, K. G. Neoh, E.-T. Kang, D. W. Pack, D. E. Leckband, *Biomaterials* **2008**, *29*, 2270.
- [128] Y.-M. Huh, Y.-w. Jun, H.-T. Song, S. Kim, J.-s. Choi, J.-H. Lee, S. Yoon, K.-S. Kim, J.-S. Shin, J.-S. Suh, J. Cheon, *J. Am. Chem. Soc.* **2005**, *127*, 12837.
- [129] M. Das, D. Mishra, T. K. Maiti, A. Basak, P. Pramanik, *Nanotechnol.* **2008**, *19*, 415101.
- [130] C.-M. Lee, H.-J. Jeong, S.-J. Cheong, E.-M. Kim, D. W. Kim, S. T. Lim, M.-H. Sohn, *Pharm. Res.* **2010**, *27*, 712.
- [131] Z. Liu, K. Chen, C. Davis, S. Sherlock, Q. Cao, X. Chen, H. Dai, *Cancer Res.* **2008**, *68*, 6652.
- [132] A. A. Bhirde, V. Patel, J. Gavard, G. Zhang, A. A. Sousa, A. Masedunskas, R. D. Leapman, R. Weigert, J. S. Gutkind, J. F. Rusling, *ACS Nano* **2009**, *3*, 307.
- [133] K. E. Scarberry, E. B. Dickerson, J. F. McDonald, Z. J. Zhang, *J. Am. Chem. Soc.* **2008**, *130*, 10258.
- [134] M. Koolpe, M. Dali, E. B. Pasquale, *J. Biol. Chem.* **2002**, *277*, 46974.
- [135] P. H. Thaker, M. Deavers, J. Celestino, A. Thornton, M. S. Fletcher, C. N. Landen, M. S. Kinch, P. A. Kiener, A. K. Sood, *Clin. Cancer Res.* **2004**, *10*, 5145.
- [136] H.-S. Cho, Z. Dong, G. M. Pauletti, J. Zhang, H. Xu, H. Gu, L. Wang, R. C. Ewing, C. Huth, F. Wang, D. Shi, *ACS Nano* **2010**, *4*, 5398.
- [137] H. Dong, Z. Zhao, H. Wen, Y. Li, F. Guo, A. Shen, F. Pilger, C. Lin, D. Shi, *Sci. China Chem.* **2010**, *53*, 2265.

- [138] K. Yang, S. Zhang, G. Zhang, X. Sun, S.-T. Lee, Z. Liu, *Nano Lett.* **2010**, *10*, 3318.
- [139] M. B. Bouchard, S. A. MacLaurin, P. J. Dwyer, J. Mansfield, R. Levenson, T. Krucker, *J. Biomed. Opt.* **2007**, *12*, 051601.
- [140] J. Mansfield, K. W. Gossage, C. C. Hoyt, R. M. Levenson, *J. Biomed. Opt.* **2005**, *10*, 041207.
- [141] Y. Inoue, K. Izawa, S. Kiryu, A. Tojo, K. Ohtomo, *Mol. Imag.* **2008**, *7*, 21.
- [142] T. Troy, D. Jekic-McMullen, L. Sambucetti, B. Rice, *Mol. Imag.* **2004**, *3*, 9.
- [143] K. C. Brown, *Curr. Pharm. Des.* **2010**, *16*, 1040.
- [144] L. R. H. Krumpke, T. Mori, *Int. J. Pept. Res. Ther.* **2006**, *12*, 79.
- [145] G. S. Shukla, D. N. Krag, *Protein Eng. Des. Sel.* **2010**, *23*, 431.
- [146] M. Böckman, M. Drosten, B. M. Pützer, *J. Gene Med.* **2005**, *7*, 179.
- [147] D. L. Jaye, F. S. Nolte, L. Mazzucchelli, C. Geigerman, A. Akyildiz, C. A. Parkos, *Am. J. Pathol.* **2003**, *162*, 1419.
- [148] E. W. Orava, N. Cicmil, J. Gariépy, *Biochim. Biophys. Acta.* **2010**, *1798*, 2190.
- [149] D. Shangguan, L. Meng, Z. C. Cao, Z. Xiao, X. Fang, Y. Li, D. Cardona, R. P. Witek, C. Liu, W. Tan, *Anal. Chem.* **2008**, *80*, 721.
- [150] V. Bagalkot, O. C. Farokhzad, R. Langer, S. Jon, *Angew. Chem. Int. Ed.* **2006**, *45*, 8149.
- [151] C. S. M. Ferreira, M. C. Cheung, S. Missailidis, S. Bisland, J. Gariépy, *Nucleic Acids Res.* **2009**, *37*, 866.
- [152] S. Wang, E. S. Humphreys, S.-Y. Chung, D. F. Delduco, S. R. Lustig, H. Wang, K. N. Parker, N. W. Rizzo, S. Subramoney, Y.-M. Chiang, A. Jagota, *Nat. Mater.* **2003**, *2*, 196.
- [153] S. Brown, T. S. Jespersen, J. Nygård, *Small* **2008**, *4*, 416.
- [154] S. Brown, *Proc. Nat. Acad. Sci. USA* **1992**, *89*, 8651.
- [155] Y. Cue, S. N. Kim, S. E. Jones, L. L. Wissler, R. R. Naik, M. C. McAlpine, *Nano Lett.* **2010**, *10*, 4559.
- [156] J. M. Slocik, J. S. Zabinski Jr., D. M. Phillips, R. R. Naik, *Small* **2008**, *4*, 548.
- [157] Z. Kuang, S. N. Kim, W. J. Crookes-Goodson, B. L. Farmer, R. R. Naik, *ACS Nano* **2010**, *4*, 452.

Received: March 7, 2011  
Revised: April 23, 2011  
Published online: June 7, 2011